Ultrafast Vibrational Frequency Shifts Induced by Electronic Excitations: Naphthols in Low Dielectric Media

Dequan Xiao,[†] Mirabelle Prémont-Schwarz,[‡] Erik T. J. Nibbering,*[,‡] and Victor S. Batista*[,†]

[†]Department of Chemistry, Yale University, P.O. Box 208107, New Haven, Connecticut 06520-8107, United States

[‡]Max Born Institut für Nichtlineare Optik und Kurzzeitspektroskopie, Max Born Strasse 2A, D-12489 Berlin, Germany

ABSTRACT: We study the solvent-induced frequency shifts of the OH-stretching mode of 1-naphthol and 2-naphthol in nonpolar/weakly polar solvents, subject to electronic excitation, with ultrafast UV/mid-infrared pump—probe spectroscopy and theoretical modeling based on Pullin's perturbative treatment of vibrational solvatochromic effects. The model is parametrized at the density functional theory (DFT) level, including the B3LYP/TZVP and TD-B3LYP/TZVP descriptions, for the naphthol chromophores in the S_0- and ^1L_b-states and accounts for both the static and the optical dielectric response of the solvent on time scales comparable to that of the OH-stretching vibrational motions. The favorable comparison between experimental and theoretical values of the solvent-induced vibrational frequency shifts suggests that the ultrafast dielectric response of the solvent contributes predominantly to the solvatochromic shifts in solvents of moderate polarity where specific solute—solvent interactions are absent.
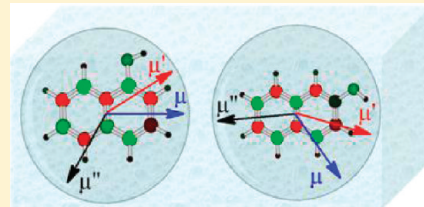
1. INTRODUCTION

Photoacidity is a term that was coined to highlight a unique property of aromatic alcohols, namely, that they show a pronounced increase in acidity upon electronic excitation.[1-6] Changes in acidity for photoacids dissolved in water range from $\Delta pK_a = pK_a(S_1) - pK_a(S_0) \approx 5-12$.[7,8] This gives rise to excited state proton transfer reactions thereby enabling studies of their ultrafast dynamics.[9-11] While much research has been devoted to proton transfer in photoacid—base complexes in the gas phase,[12-17] recent experimental and theoretical evidence support hydrogen transfer mechanisms instead of the expected proton transfer, with a net electron and proton transfer with bases like amines.[18-20] In contrast, photoacids typically release a proton in solvents with a high dielectric constant, most notably in water.[21] To understand such net separation of the positive solvated proton and the negatively charged photobase, solvation of the reaction products must be of major importance.[22] As such, to explain photoacidity one should not only aim for a quantitative determination of the intrinsic electronic density effects affected by photoexcitation[23-25] but also for a full exploration of the microscopic parameters governed by solvation. Studying the coupling between the electronic and nuclear degrees of freedom of a solute embedded in a solvent by UV/vis spectroscopy is well established.[26-28] Solvation of photoacid molecules has been investigated using electronic spectroscopy and analyzed with semiempirical descriptions based on linear free energy relationships, such as the Kamlet—Taft approach.[29-32] However, solvation can also be probed by looking at the frequency position of the vibrations of a solute,[33-36] where the solvatochromic frequency shifts are typically 2 orders of magnitude smaller than those observed by electronic spectroscopy. The hydrogen stretching vibrations of the proton donating hydroxyl OH or (protonated) amine NH_3^+ groups would provide a direct insight into the local interactions of photoacid molecules.

We present experimental and theoretical results of transient IR spectroscopy of the OH-stretching mode of 1-naphthol (1N) and 2-naphthol (2N) (see Scheme 1), the two prototype photoacids.[37-39] In order to understand the basic intrinsic electronic charge redistribution as well as solute—solvent couplings, we first discuss results in solvents of low polarity, where specific solute—solvent interactions, i.e., hydrogen bonds, are understood not to take place. Quantum chemical calculations on 1N and 2N are presented to estimate the changes in electron density distributions caused by electronic excitation. We then analyze the solute—solvent couplings by the Onsager solvation model, where the solute is represented by a point dipole embedded in a spherical Onsager cavity interacting with a dielectric continuum representing the surrounding solvent molecules.[40-44] While the experimental vibrational frequency shifts for weakly hydrogen bonded molecular systems in the electronic ground state have been linked to a perturbation theory of the solvated oscillator potential,[45-47] no such relationship describing how the observed frequency shifts are related to molecular parameters exists for the excited state. We follow the (steady-state) perturbative description by Pullin[43-47] and refine it with the time-dependent theory by van der Zwan and Hynes[48] to take into account the effects of solvent shell rearrangements. We then compare the experimentally measured solvent-induced OH stretching frequency shifts of 1N in the S_0- and S_1-states with theoretical predictions using quantum chemical calculations, as well as with previously reported results obtained on 2N.[49] Finally, we discuss the differences observed between 1N and 2N.
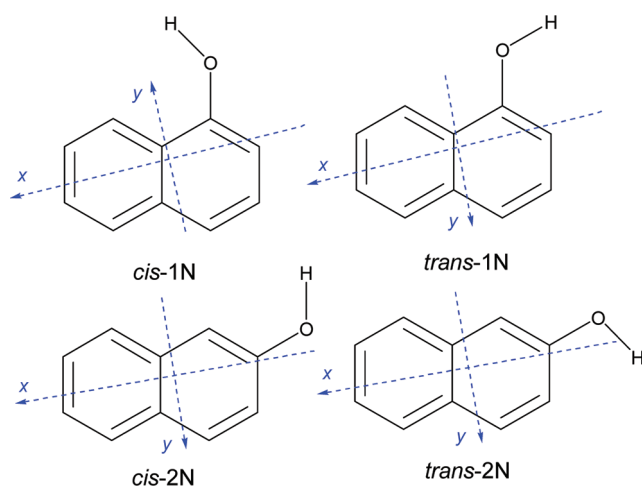
Scheme 1. Chemical Structures of *cis* and *trans* Conformers of 1N and 2N

2. METHODS: THEORY AND EXPERIMENT

2.1. Computational Methods. Geometry optimization and calculations of ground state molecular properties, including electronic energies, transition dipole moments, electrostatic potential (ESP) atomic charges, dipole moments, dipole derivatives with respect to normal modes, vibrational normal modes, and solvation energies were obtained at the DFT (B3LYP/ TZVP) level of theory, as implemented in Gaussian 09.[50] Analogous excited state calculations were performed at the TD-DFT (B3LYP/TZVP) level. The polarizable continuum model (PCM) was used for computations of solvation energies and for geometry optimization in dielectric continuum media. The order of the excited states, ^1L_a and ^1L_b, in the energy ladder of both the *cis*- and *trans*-rotamers of 1N or 2N was found to be switched with respect to the energetic order probed by experiments.[15,51] This behavior was studied previously and attributed to an underestimation of the interaction between ionic components in the ^1L_a-state due to the improper asymptotic form of standard functionals.[52] However, the distinct electronic symmetry of these states enabled us to identify the ^1L_b state and compute the molecular parameters in this state at the TD-DFT level, including dipole moments as well as the first and second dipole derivatives.

The anharmonic force constant and the harmonic constant were calculated by the anharmonic vibrational analysis implemented in the Gaussian 09 program using the keyword freq(= anharmonic). For the anharmonic vibrational analysis, the HF/6-31g method was used for the ground state, and the CIS/6-31g method was used for the excited state. Once the first derivatives of the dipole moment with respect to the kth normal mode ($\mu'_k = \partial\mu/\partial Q$) were calculated by the keyword IOP(7/33 = 1) in Gaussian 09, the second dipole moment derivatives were computed as follows:

$$\mu''_k = \frac{\partial(\mu'_k)}{\partial Q} = \sum_i \frac{\partial(\mu'_k)}{\partial x_i} l_{ik} \qquad (1)$$

where l_{ik} is the transformation matrix from the Cartesian coordinate to the normal mode coordinate, and the derivative in the Cartesian coordinate $\partial(\mu'_k)/(\partial x_i)$ was calculated

numerically by finite differences

$$\frac{\partial(\mu'_k)}{\partial x_i} = \frac{\mu'_k(x_i + \delta x_i) - \mu'_k(x_i - \delta x_i)}{2\delta x_i} \qquad (2)$$

2.2. Experimental Methods. 1-Naphthol (99%), 2-naphthol (99%), *n*-hexane, cyclohexane, C_2Cl_4, $CHCl_3$, CH_2Cl_2, and 1,2-dichloroethane (Reagent Plus; ≥99%) were all purchased from Aldrich. Steady-state electronic absorption spectra were recorded with a double-beam UV/vis spectrometer (Perkin-Elmer), and emission spectra were recorded with a spectrofluorometer (Spex Fluorolog).

We observe a significantly lower emission quantum yield and a deviation of the emission band shape compared to that of the other solvents in $CHCl_3$ and C_2Cl_4 (total fluorescence quenching was observed in CCl_4), which unfortunately precludes the precise determination of the electronic Stokes shift in these solvents. The quenching behavior of some halocarbon solvents with naphthalene and its derivatives has previously been reported in the literature[53,54] and is tentatively ascribed to a special exciplex interaction between these halocarbon solvents and the aromatic system in the S_1-state, thereby shortening the electronic excited state lifetime.

Ultrafast infrared spectra were recorded using an experimental setup described previously.[55] Electronic excitation of 1N and 2N was achieved with pulses (3 μJ, 50 fs) generated by sum frequency mixing of the fundamental of a 1 kHz amplified Ti: sapphire laser (Tsunami oscillator with Spitfire Pro regenerative and booster amplifier stages; Spectra Physics) and visible pulses generated by a noncollinear optical parametric amplifier (NOPA). The excitation wavelength was tuned to the lowest energy peak of the ^1L_b transition for each solvent thereby ensuring minimal excess energy (318 to 330 nm). The pump pulses were sent to a delay line and then focused onto the sample with a beam diameter of approximately 200 μm. Tunable mid-infrared pulses were generated by a double-pass optical parametric amplification followed by difference frequency mixing of signal and idler. The probe and reference pulses were obtained using reflections from a ZnSe wedge and focused onto the sample by means of an off-axis parabolic mirror (focal diameter, 150 μm). The probe and reference pulses were dispersed in a polychromator (8–10 cm^{-1} resolution), and spectrally resolved absorbance changes were recorded simultaneously for each shot using a liquid nitrogen cooled HgCdTe double array detector (2 × 31 pixels). The time resolution was determined to be 150 fs based on the cross-correlation between the UV-pump and IR-probe pulses measured in a ZnSe semiconductor placed at the sample position. A peristaltic pump was used to circulate the sample through a flow cell (1 mm thick CaF2 windows separated by a 300 μm thick Teflon spacer) to guarantee that a new sample volume was excited for every laser shot. Concentrations of only 20 mM were used in order to minimize the self-association found to occur in the nonpolar solvents such as *n*-hexane or cyclohexane. In addition, given the formation of a photoproduct sticking to the cell window, a well-known phenomenon in aromatic systems with electron donating substituents,[56,57] the sample holder was moved up and down during the measurement. Also, the electronic and steady-state infared spectra were monitored before and after the measurement to ensure that the nature of the solution did not change.

The solutions used in the experiments were checked for water contamination. Furthermore, the effect of water was verified through a controlled experiment where known quantities of water were added to a solution of 1N in CH_2Cl_2. It was found that the complexation constant was quite small and that water did not change the nature of the OH-stretching band of uncomplexed 1N.

3. SOLVENT-INDUCED VIBRATIONAL FREQUENCY SHIFTS: PULLIN−VAN DER ZWAN−HYNES PERTURBATIVE APPROACH

Theoretical descriptions of solvent-induced vibrational frequency shifts have often relied on a perturbative approach, where the solute−solvent interaction is treated as a perturbation to the vibrational Hamiltonian of a gas phase molecule.[58] When a detailed microscopic description of the solute−solvent interaction is not available, solvent continuum models are of use. Kirkwood[59] and Bauer and Magat[60] were the first to use the Onsager reaction field model of a point dipole representing the solute embedded in a spherical cavity surrounded by a continuous solvent medium characterized by a macroscopic dielectric constant. Pullin generalized this perturbative approach for polyatomic polarizable molecules with anharmonic vibrational potentials, dissolved in a continuum solvent with a frequency-dependent dielectric constant.[43,44] Buckingham similarly used an explicit quantum chemical treatment of a diatomic molecule embedded in a continuum solvent with a frequency-dependent dielectric constant.[40−42] His analytical expressions for solvent-induced vibrational frequency shifts have been used extensively and refined by others.[61,62] They enable the relative contributions of solvent polarity (ε_0) and solvent polarizability at optical frequencies (ε_∞) to be estimated. Recently, this approach has been applied to weakly hydrogen-bonded cases.[45−47]

Pullin's and Buckingham's derivations are closely related, except for the starting points in defining molecular Hamiltonians and the estimation of the dielectric constants for different contributions in the expressions for the solvent-induced vibrational frequency shifts. However, while the microscopic meaning of the different constants in Buckingham's expressions is not straightforward for polyatomic molecules,[63] Pullin's expression makes the extension to polyatomic molecules with off-diagonal anharmonicities straightforward. We therefore apply Pullin's derivation of the solvent-induced vibrational frequency shifts, and extend it with the van der Zwan−Hynes relationship[48] to describe a time-dependent reaction field induced by the point dipole altered by electronic excitation.[33−35] Even though we discuss solvent-induced frequency shifts of 1N and 2N in solvents without explicit hydrogen bonding of the OH-group, this approach can be extended to hydrogen bonding solvents as well, provided that a proper expression for the vibrational potential of the OH-stretching modes of hydrogen-bonded complexes can be defined.

In the following, we present the analytical expressions for the time-dependent solvent-induced vibrational frequency shift, following the derivation of Pullin[43,44] and the time-dependent extension as defined by van der Zwan and Hynes.[48]

3.1. Morse Potential. The Morse vibrational potential in the gas phase of the molecular system $V_i(Q)$ can be written as a Taylor expansion along vibrational coordinate Q as

$$V_i(Q) = D_i(1 - e^{-\alpha_i Q})^2$$

$$= \frac{1}{2!}V_i'' Q^2 + \frac{1}{3!}V_i''' Q^3 + \dots \tag{3}$$

where D_i is the dissociation energy of the ith electronic state, and

$\alpha_i = (V_i''/2D_i)^{1/2}$. Note that for uncomplexed 1N or 2N, we assume that the anharmonic coupling between the OH-stretching mode with the other normal modes (i.e., cubic force constants V_i''') can be discarded in the Taylor expansion of eq 3. For this, we rely on the large body of information accumulated with ultrafast infrared spectroscopy of vibrational modes in liquid solution,[64−71] where the vibrational dephasing and vibrational relaxation rates can be properly explained with an anharmonic OH-stretching mode coupled to a heat bath comprising overdamped low-frequency solvent modes.[72,73] The quadratic force constant V_i'' and cubic force constant V_i''' of the Morse potential are then

$$V_i'' = 2D_i\alpha_i^2 \tag{3a}$$

$$V_i''' = -6D_i\alpha_i^2 \tag{3b}$$

3.2. Solvation of Morse Potential by the Onsager Point−Dipole Model. The dielectric response of the medium surrounding the spherical Onsager cavity (with a radius a_i) formed by the polar photoacid molecule results in a reaction field $\mathbf{R}_i(Q)$ that interacts with the molecule. The solvation energy is

$$V_s(Q) = -\frac{1}{2}\boldsymbol{\mu}_i(Q)\mathbf{R}(Q)$$

$$= V_s^0 + V_s'Q + \frac{1}{2!}V_s''Q^2 + \dots \tag{4}$$

where $\boldsymbol{\mu}_i(Q)$ is the molecular dipole moment, that is dependent on the nuclear coordinate Q. Using a Taylor expansion along the normal coordinate, this becomes

$$\boldsymbol{\mu}_i(Q) = \boldsymbol{\mu}_i^0 + \boldsymbol{\mu}_i'Q + \boldsymbol{\mu}_i''Q^2 + \dots \tag{4a}$$

where $\boldsymbol{\mu}_i^0$ is the permanent dipole moment of the solute, with $\boldsymbol{\mu}_i'$ and $\boldsymbol{\mu}_i''$ being the first and second derivatives of the dipole moment along the vibrational coordinate Q, respectively. The reaction field then becomes

$$\mathbf{R}_i(Q) = f_0\boldsymbol{\mu}_i^0 + f_\infty\boldsymbol{\mu}_i'Q + f_\infty\boldsymbol{\mu}_i''Q^2 + \dots \tag{4b}$$

where f_0 and f_∞ are the functions of the static dielectric constant ε_0 and the optical dielectric constant ε_∞, respectively.

$$f_0 = \frac{1}{a_i^3}\left(\frac{2\varepsilon_0 - 2}{2\varepsilon_0 + 1}\right) = \frac{1}{a_i^3}F_0 \tag{4c}$$

$$f_\infty = \frac{1}{a_i^3}\left(\frac{2\varepsilon_\infty - 2}{2\varepsilon_\infty + 2}\right) = \frac{1}{a_i^3}F_\infty \tag{4d}$$

The optical dielectric function f_∞ is related to the static dielectric function f_0 by

$$f_\infty = f_0 + f'(Q - Q^*) \tag{4e}$$

where Q^* is the new equilibrium bond length of the Morse potential in solution. From the equations presented above, the following quantities can be readily identified:

$$f_{or} = f_0 - f_\infty \tag{4f}$$

$$F_0 = \frac{2\varepsilon_0 - 2}{2\varepsilon_0 + 1} \tag{4g}$$

$$F_\infty = \frac{2\varepsilon_\infty - 2}{2\varepsilon_\infty + 2} \tag{4h}$$

Substituting eqs 4a and 4b into eq 4, we obtain

$$V_s(Q) = -\frac{1}{2}(\boldsymbol{\mu}_i^0 + \boldsymbol{\mu}_i' Q + \boldsymbol{\mu}_i'' Q^2 + ...)(f_0\boldsymbol{\mu}_i^0$$
$$+ f_\infty\boldsymbol{\mu}_i' Q + f_\infty\boldsymbol{\mu}_i'' Q^2 + ...) \tag{5}$$

By grouping terms by order Q and comparing them to the Taylor expansion coefficients, we find

$$V_s' = -\frac{1}{2}(f_0 + f_\infty)\boldsymbol{\mu}_i^0 \cdot \boldsymbol{\mu}_i' \tag{5a}$$

According to eq 4e, at the equilibrium point in solution ($Q = Q^*$), $f_\infty = f_0$, one finds

$$V_s'\Big|_{Q=Q^*} = -f_0\boldsymbol{\mu}_i^0 \cdot \boldsymbol{\mu}_i' \tag{5b}$$

$$V_s'' = -[(f_0 + f_\infty)\boldsymbol{\mu}_i^0 \cdot \boldsymbol{\mu}_i'' + f_\infty\boldsymbol{\mu}_i' \cdot \boldsymbol{\mu}_i'] \tag{5c}$$

The solvated Morse potential then becomes

$$V_{sol}(Q) = V_i(Q) + V_s(Q)$$
$$= \frac{1}{2!}V_i'' Q^2 + \frac{1}{3!}V_i''' Q^3 + V_s^0 + V_s' Q$$
$$+ \frac{1}{2!}V_s'' Q^2 + ... \tag{6}$$

The first derivative of $V_{sol}(Q)$ is

$$V_{sol}'(Q) = V_s' + V_i'' Q + V_s'' Q + \frac{1}{2}V_i''' Q^2 + ... \tag{7}$$

At the new equilibrium point

$$V_{sol}'(Q)|_{Q=Q^*} = 0 \tag{8}$$

and thus, the new equilibrium length Q^* is

$$Q^* \approx -\frac{V_s'}{V_i'' + V_s''}\Big|_{Q=Q^*} \approx -\frac{V_s'\Big|_{Q=Q^*}}{V_i''} \tag{9}$$

The second derivative of $V_{sol}(Q)$ is

$$V_{sol}''(Q) = V_i'' + V_i''' Q + V_s'' + ... \tag{10}$$

By substituting eq 7 into eq 8, we obtain

$$V_{sol}''(Q^*) \approx V_i'' - V_i''' \frac{V_s'\Big|_{Q=Q^*}}{V_i''} + V_s'' \tag{10a}$$

$$= V_i''\left[1 - \frac{1}{V_i''}\left(\frac{V_i'''}{V_i''}V_s'\Big|_{Q=Q^*} - V_s''\right)\right] \tag{10b}$$

By substituting eqs 5a and 5b into eq 10b, we obtain

$$V_{sol}'' = V_i''\left\{1 - \frac{1}{V_i''}\left[f_0\left(\boldsymbol{\mu}_i'' \cdot \boldsymbol{\mu}_i^0 - \frac{V_i'''}{V_i''}\boldsymbol{\mu}_i' \cdot \boldsymbol{\mu}_i^0\right)\right.\right.$$
$$\left.\left. + f_\infty(\boldsymbol{\mu}_i'' \cdot \boldsymbol{\mu}_i^0 + \boldsymbol{\mu}_i' \cdot \boldsymbol{\mu}_i')\right]\right\} \tag{11}$$

$$= V_i''(1 - \Delta) \tag{11a}$$

where

$$\Delta = \frac{1}{V_i''}\left[f_0\left(\boldsymbol{\mu}_i'' \cdot \boldsymbol{\mu}_i^0 \frac{V_i'''}{V_i''}\boldsymbol{\mu}_i' \cdot \boldsymbol{\mu}_i^0\right) + f_\infty(\boldsymbol{\mu}_i'' \cdot \boldsymbol{\mu}_i^0 + \boldsymbol{\mu}_i' \cdot \boldsymbol{\mu}_i')\right] \tag{11b}$$

3.3. Vibrational Frequency Shifts Due to Solvation. We are now able to define the solvent-induced vibrational frequency shift as

$$\frac{\Delta\nu_i}{\nu_0^i} \equiv \frac{\nu_0^i - \nu_s^i}{\nu_0^i} = \sqrt{\frac{V_i'' - V_i''(1 - \Delta)}{V_i''}} \approx \Delta/2 \tag{12}$$

where $\Delta\nu_0^i = \nu_0^i - \nu_s^i$ is the difference between the vibrational frequency in solution (ν_s^i) and in the gas phase (ν_0^i). By substituting eq 11b into eq 12, we obtain

$$\frac{\Delta\nu_i}{\nu_0^i} = \frac{f_0}{2V_i''}\left(\boldsymbol{\mu}_i'' \cdot \boldsymbol{\mu}_i^0 - \frac{V_i'''}{V_i''}\boldsymbol{\mu}_i' \cdot \boldsymbol{\mu}_i^0\right)$$
$$+ \frac{f_\infty}{2V_i''}(\boldsymbol{\mu}_i'' \cdot \boldsymbol{\mu}_i^0 + \boldsymbol{\mu}_i' \cdot \boldsymbol{\mu}_i') \tag{13}$$

$$= \frac{f_{or}}{2V_i''}\mathbf{g}_i\boldsymbol{\mu}_i^0 + \frac{f_\infty}{2V_i''}[(\mathbf{g}_i + \boldsymbol{\mu}_i'')\boldsymbol{\mu}_i^0 + \boldsymbol{\mu}_i' \cdot \boldsymbol{\mu}_i'] \tag{13a}$$

where

$$\mathbf{g}_i = \boldsymbol{\mu}_i'' - \frac{V_i'''}{V_i''}\boldsymbol{\mu}_i' \tag{13b}$$

Substituting eqs 4c–d and $V_i'' = k = 4\pi^2 m\nu_0^2$ into eq 13, we find that $\Delta\nu$ shows a linear dependence on F_0

$$\Delta\nu_i = \frac{F_0}{8\pi^2 m\nu_0^i a_i^3}\left(\boldsymbol{\mu}_i^0 \cdot \boldsymbol{\mu}_i'' \frac{V_i'''}{V_i''}\boldsymbol{\mu}_i^0 \cdot \boldsymbol{\mu}_i'\right)$$
$$+ \frac{F_\infty}{8\pi^2 m\nu_0^i a_i^3}(\boldsymbol{\mu}_i' \cdot \boldsymbol{\mu}_i' + \boldsymbol{\mu}_i^0 \cdot \boldsymbol{\mu}_i'') \tag{14}$$

The slope of this linear relationship between $\Delta\nu$ and F_0 is given by

$$S_i = \frac{F_0}{8\pi^2 m\nu_0^i a_i^3}\left(\boldsymbol{\mu}_i^0 \cdot \boldsymbol{\mu}_i'' - \frac{V_i'''}{V_i''}\boldsymbol{\mu}_i^0 \cdot \boldsymbol{\mu}_i'\right) \tag{14a}$$

and the intercept is derived to be

$$B_i = \frac{F_\infty}{8\pi^2 m\nu_0^i a_i^3}(\boldsymbol{\mu}_i' \cdot \boldsymbol{\mu}_i' + \boldsymbol{\mu}_i^0 \cdot \boldsymbol{\mu}_i'') \tag{14b}$$

Formally, F_∞ is also solvent-dependent, as the dielectric constant at optical frequencies is related to the refractive index through the relationship $\varepsilon_\infty = n^2$. However, the variation of the refractive

Table 1. Dielectric Constants and Refractive Indices for the Solvents Used in This Study

solvents	ε_0 (lit)[a]	n (lit)[a]	n (3337 cm^{-1}) ± 0.015	ε_∞ (3337 cm^{-1})
n-hexane	1.8799	1.3723	1.418	2.011
c-hexane	2.0243	1.4235	1.455	2.117
C_2Cl_4	2.28	1.5032	1.457	2.123
$CHCl_3$	4.806	1.4429	1.408	1.982
CH_2Cl_2	8.93	1.4212	1.379	2.020
1,2-DCE	10.0	1.4138	1.408	1.982

[a] Values taken from ref 97.
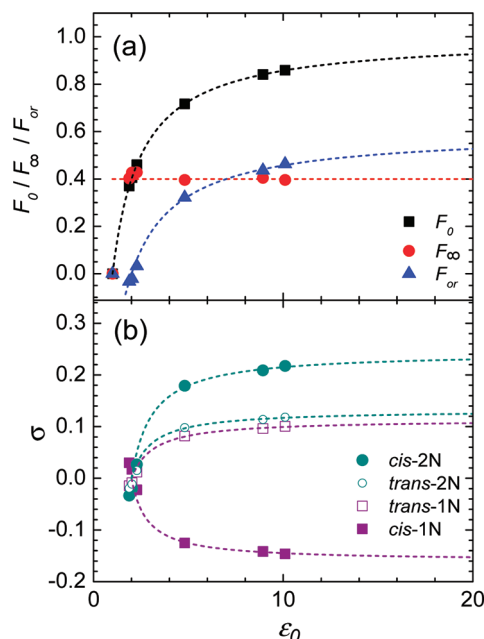
Figure 1. (a) Dependence of F_0, F_∞, and F_{or} on the static dielectric constant ε_0. (b) Dependence of the frequency shift ratio σ on the static dielectric constant ε_0.

index n at optical frequencies is rather small. This is true for both electronic and vibrational transitions, provided solvent resonances are not close to those of the solute. In order to confirm our assumption on ε_∞, we have measured the group delay of femtosecond mid-infrared pulses through a flow cell with a fixed thickness filled with the solvents used in this study. As shown in Table 1, the solvent dependence of n_{IR} at 3 μm is minor, and thus considering F_∞ to be constant is a valid approximation (see Figure 1).

3.4. Frequency Shifts of the Solvated Ground State. Since the steady-state expression by Pullin is applicable for the OH-stretching mode of 1N and 2N in the electronic ground state, we can, according to eqs 13 and 14, define the following:

$$\Delta \nu_g = \frac{F_0}{8\pi^2 m \nu_0^g a_g{}^3} \left(\boldsymbol{\mu}_g'' \cdot \boldsymbol{\mu}_g^0 - \frac{V_g'''}{V_g''} \boldsymbol{\mu}_g' \cdot \boldsymbol{\mu}_g^0 \right) + \frac{F_\infty}{8\pi^2 m \nu_0^g a_g{}^3} (\boldsymbol{\mu}_g' \cdot \boldsymbol{\mu}_g' + \boldsymbol{\mu}_g'' \cdot \boldsymbol{\mu}_g^0) \tag{15}$$

$$S_g = \frac{1}{8\pi^2 m \nu_0^g a_g{}^3} \left(\boldsymbol{\mu}_g'' \cdot \boldsymbol{\mu}_g^0 - \frac{V_g'''}{V_g''} \boldsymbol{\mu}_g' \cdot \boldsymbol{\mu}_g^0 \right) \tag{16}$$

3.5. Vibrational Frequency Shifts Due to Electronic Excitations. For the OH-stretching mode of 1N and 2N in the electronic excited state, we have to consider the role of solvent reorganization (solvation dynamics) expected to take place on ultrafast time scales. Ultrafast solvation dynamics of solute chromophores is a topic that has been extensively explored during the past several decades.[26−28,74−76] Electronic excitation of a solute implies the rearrangement of electronic charge density within the solute chromophore. Because of the solute−solvent coupling, the surrounding solvent shells respond to this electronic excitation with an instantaneous component due to the electronic hyperpolarizability and noninstantaneous components due to nuclear dynamics. A multitude of models with different degrees of sophistication have been developed to describe the time-dependent solvent reorganization.[28] We follow the established van der Zwan−Hynes approach[48] to incorporate a time-dependent reaction field into the expressions for the time-dependent solvent-induced vibrational frequency shifts upon electronic excitation of a solute.

$$\mathbf{R}_i(t) = f_\infty \boldsymbol{\mu}_e(Q) + f_{or} \boldsymbol{\mu}(t) \tag{17}$$

where

$$\boldsymbol{\mu}(t) = \boldsymbol{\mu}_g^0(1 - z(t)) + \boldsymbol{\mu}_e^0 z(t) \tag{17a}$$

In this expression, the time-dependent dipole moment $\boldsymbol{\mu}(t)$ takes into account the finite dielectric response of the solvent by a time-dependent change from $\boldsymbol{\mu}_g^0$ to $\boldsymbol{\mu}_e^0$, where $\boldsymbol{\mu}_e^0$ and $\boldsymbol{\mu}_g^0$ are the permanent dipole moments in the electronic excited and ground states, respectively. $z(t)$ is the solvation coordinate changing from $z(t = 0) = 0$ at the initial solvent configuration of the chromophore in the S_0-state, to $z(t = \infty) = 1$, when the equilibrium solvent configuration for the chromophore in the S_1-state has been reached. The following solvation correlation function $C(t)$ is connected to the time-dependent solvation coordinate $z(t)$:[33−35]

$$C(t) = \frac{\Delta \nu_s^e(t) - \Delta \nu_s^e(t = \infty)}{\Delta \nu_s^e(t = 0) - \Delta \nu_s^e(t = \infty)} = 1 - z(t) \tag{18}$$

Replacing $\boldsymbol{\mu}_e(Q)$ in eq 17 using eq 4a, we find

$$\mathbf{R}(t) = f_\infty (\boldsymbol{\mu}_e^0 \cdot \boldsymbol{\mu}_e' Q + \boldsymbol{\mu}_e'' Q^2 + ...) + f_{or} \boldsymbol{\mu}(t) \tag{19}$$

By replacing eq 4b by eq 19 and performing a derivation similar to that in eqs 5−13, we obtain the following time-dependent solvent-dependent vibrational frequency shift:

$$\frac{\Delta \nu(t)}{\nu_0^e} = \frac{f_\infty}{2V_e''} [(\mathbf{g}_e + \boldsymbol{\mu}_e'') \boldsymbol{\mu}_e^0 + \boldsymbol{\mu}_e' \cdot \boldsymbol{\mu}_e']$$
$$+ \frac{f_{or}}{2V_e''} \mathbf{g}_e \boldsymbol{\mu}(t) \tag{20}$$

At long delay times, solvent shell reorganization is fully established, i.e., when $z(t = \infty) = 1$, so we can simplify using $\boldsymbol{\mu}(t) = \boldsymbol{\mu}_e^0$ giving

$$\Delta \nu_e = \frac{F_0}{8\pi^2 m \nu_0^e a_e{}^3} \left(\boldsymbol{\mu}_e'' \cdot \boldsymbol{\mu}_e^0 - \frac{V_e'''}{V_e''} \boldsymbol{\mu}_e' \cdot \boldsymbol{\mu}_e^0 \right)$$
$$+ \frac{F_\infty}{8\pi^2 m \nu_0^e a_e{}^3} (\boldsymbol{\mu}_e' \cdot \boldsymbol{\mu}_e' + \boldsymbol{\mu}_e'' \cdot \boldsymbol{\mu}_e^0) \tag{21}$$

2779

dx.doi.org/10.1021/jp208426v |J. Phys. Chem. A 2012, 116, 2775−2790

$$S_e = \frac{1}{8\pi^2 m v_0^e a_e{}^3}\left(\boldsymbol{\mu}_e'' \cdot \boldsymbol{\mu}_e^0 - \frac{V_e'''}{V_e''}\boldsymbol{\mu}_e' \cdot \boldsymbol{\mu}_e^0\right) \quad (22)$$

3.6. Ratio of Vibrational Frequency Shifts: Excited State/ Ground State. To summarize, the solvent-dependent vibrational frequency shift of the OH-stretching marker mode of 1N or 2N in electronic state i can be approximated as a linear function of F_0 with a slope S_i governed by molecular parameters V_i'', V_i''', $\boldsymbol{\mu}_i^0$, $\boldsymbol{\mu}_i'$, and $\boldsymbol{\mu}_i''$ as well as the Onsager cavity size a_i. In the derivation, the vectorial properties of the molecular dipole moment and its derivatives are taken into account. As the molecular parameters of the solute vibrational potential (V_i'' and V_i''') and solute dipole moment ($\boldsymbol{\mu}_i^0$, $\boldsymbol{\mu}_i'$, and $\boldsymbol{\mu}_i''$) in electronic state i can be calculated with ab initio quantum chemical methods, and the Onsager cavity size a_i can be estimated within Onsager's reaction field theory, one can then calculate the absolute solvent-dependent vibrational frequency shifts by using eq 15 for the S_0-state and eqs 20 or 21 for the time-dependent and long time values for the S_1-state. We will compare the experimental values obtained for the solvent-dependent frequency shifts for the OH-stretching modes of 1N and 2N with theoretical predictions using the above-defined formalism in section 5. Here, it is useful to compare experimental and theoretical values for the ratio of slopes in the plot of $\Delta\nu$ as a function of F_0 for 1N or 2N in the electronic excited state to that in the ground state. From eqs 22 and 16, we derive

$$\frac{S_e}{S_g} = \frac{\left(\boldsymbol{\mu}_e'' \cdot \boldsymbol{\mu}_e^0 - \dfrac{V_e'''}{V_e''}\boldsymbol{\mu}_e' \cdot \boldsymbol{\mu}_e^0\right)}{\boldsymbol{\mu}_g'' \cdot \boldsymbol{\mu}_g^0 - \dfrac{V_g'''}{V_g''}\boldsymbol{\mu}_g' \cdot \boldsymbol{\mu}_g^0}\frac{\nu_0^g}{\nu_0^e}\left(\frac{a_g}{a_e}\right)^3 \quad (23)$$

where the Onsager cavity radius a_i can be derived from the Onsager solvation energy V_S^i as follows:

$$V_S^i = -\frac{\mu_i{}^2}{a_i{}^3}\frac{F_0}{2} \quad (23a)$$

In addition to that, the relative importance of instantaneous vs noninstantaneous contributions in the time-dependent vibrational frequency shift in the electronic excited state can be estimated from the ratio of the early time-dependent shift ($t = 0$) vs the long time shift ($t = \infty$)

$$\sigma \equiv \frac{\Delta\nu_s^e(t=0) - \Delta\nu_s^e(t=\infty)}{\Delta\nu_s^e(t=\infty)}$$

$$= \frac{(F_0 - F_\infty)\left[\boldsymbol{\mu}_e'' - \dfrac{V_e'''}{V_e''}\boldsymbol{\mu}_e'\right]\cdot[\boldsymbol{\mu}_g^0 - \boldsymbol{\mu}_e^0]}{F_0\left[\boldsymbol{\mu}_e'' - \dfrac{V_e'''}{V_e''}\boldsymbol{\mu}_e'\right]\cdot\boldsymbol{\mu}_e^0 + F_\infty[\boldsymbol{\mu}_e'' \cdot \boldsymbol{\mu}_e^0 + \boldsymbol{\mu}_e' \cdot \boldsymbol{\mu}_e']} \quad (24)$$

4. RESULTS

4.1. Nature of Electronic Excitation to the ^1L_b-State. The two lowest-lying electronic transitions for naphthalene were determined by Platt and designated as ^1L_a and ^1L_b (see Figure 2).[51] The transition dipole moments of these two electronic excitations are polarized perpendicularly to each other. The ^1L_a-transition dipole
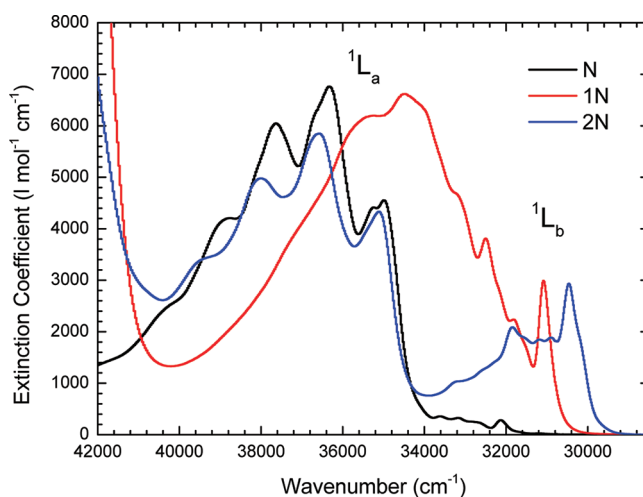
Figure 2. UV/vis electronic absorption spectra of naphthalene (N), 1-naphthol (1N), and 2-naphthol (2N) in *n*-hexane, showing the location of the ^1L_a- and ^1L_b-manifolds.

moment is oriented through the short-axis along the central C–C bond connecting the two aromatic rings, and the forbidden ^1L_b-transition dipole points along the long through-bond axis. The addition of an OH-group at the α- or β-position to form 1N or 2N breaks the symmetry, thereby mixing the two electronic states with a concomitant change in relative energy spacing and in relative magnitudes of transition dipole moments.[77] In 1N, one observes a large spectral overlap between the two transitions. The origin absorption transition to the S_1-state (^1L_b) is located at 31 095 cm^{-1}, whereas the electronic absorption band of the S_2-state (^1L_a) starts in the region around 33 200 cm^{-1}. For 2N, the first two electronic excited singlet states are clearly separated in energy. The origin absorption of the $S_0 \rightarrow S_1$ ($S_0 \rightarrow {}^1L_b$) transition of 2N is located at 30 342 cm^{-1} in *n*-hexane, whereas the second $S_0 \rightarrow S_2$ ($S_0 \rightarrow {}^1L_a$) electronic transition is reached at 35 137 cm^{-1}.

We now present results from the quantum chemical calculations of the electronic ground and excited states of 1N and 2N. We have to distinguish between two possible stable rotamer geometries with different orientations of the O–H bond vector relative to the aromatic ring, denoted as *cis*- and *trans*-, respectively. Previous calculations have shown that while the nature of the electronic transitions of naphthalene is conserved for 1N, in 2N, significant mixing between the two states occurs.[38] Our quantum chemical calculations of the electronic ground and excited states of 1N and 2N support these findings. The ^1L_b excited state obtained from our TD-DFT calculations is identified by referring to the orientation of the electronic transition moments and the corresponding oscillator strengths, as well as the composite configurations of the excited state wave functions. The TD-DFT(B3LYP/TZVP) calculations (see Table 2) show that for both *cis*- and *trans*-1N, the electronic $S_0 \rightarrow {}^1L_b$ transition dipole moment is polarized close to the direction of the long-axis of the naphthalene ring. For both *cis*- and *trans*-2N, however, the $S_0 \rightarrow {}^1L_b$ transition dipole moment is polarized slightly tilted away from the short-axis of the naphthalene ring. In contrast, the $S_0 \rightarrow {}^1L_a$ transition dipole moment is always directed along the short-axis of the naphthalene ring for any rotamer of both 1N and 2N. The oscillator strength of the $S_0 \rightarrow {}^1L_b$ electronic transition is much smaller than that of the $S_0 \rightarrow {}^1L_a$ transition. The calculated orientation of the electronic transition dipole moment and oscillator strengths are summarized in

Table 2. Transition Dipole Moments of 1N and 2N, with the Oscillator Strength *f*, Calculated by TD-DFT at the B3LYP/TZVP Level
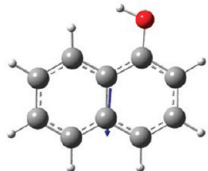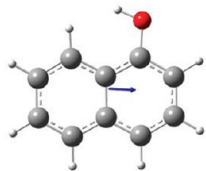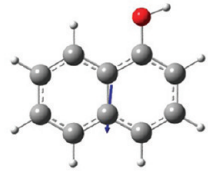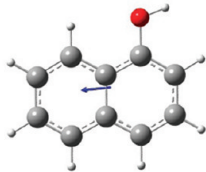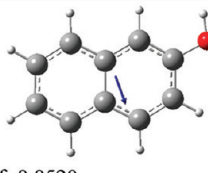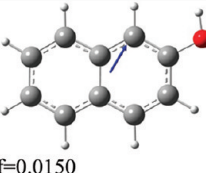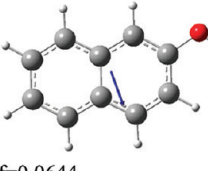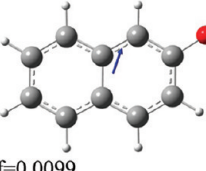
	$S_0 \rightarrow {}^1L_a$	$S_0 \rightarrow {}^1L_b$
cis-1N	f=0.0666	f=0.0236
trans-1N	f=0.0738	f=0.0271
cis-2N	f=0.0520	f=0.0150
trans-2N	f=0.0644	f=0.0099

Table 2. These findings are consistent with experimental and theoretical studies reported in the literature,[38,78,79] despite a discrepancy in calculated ordering of energy of the ${}^1L_a$- and ${}^1L_b$-states.[52]

In Table 3, we compare the electronic configurations of the HOMO $-$ 1 (ψ_{H-1}), HOMO (ψ_H), LUMO (ψ^*_L), and LUMO + 1 (ψ^*_{L+1}) molecular orbitals of the *cis*- and *trans*-rotamers of 1N and 2N as well as those of naphthalene. It appears that for both 1N and 2N, the ${}^1L_a$-state is to a large degree dominated by the $\psi_H \psi_L^*$ configuration, whereas the ${}^1L_b$-state is composed of the antisymmetric combination of the $\psi_{H-1}\psi_L^*$ and $\psi_H\psi_{L+1}^*$ configurations. These observations are consistent with numerical studies reported in the literature based on calculations at the Hückel or empirical CI levels.[38,78]
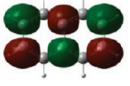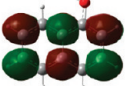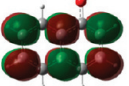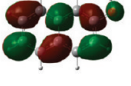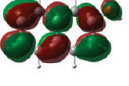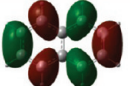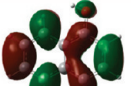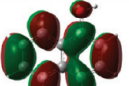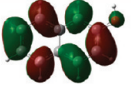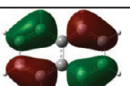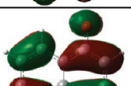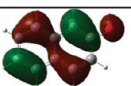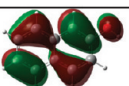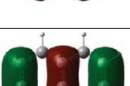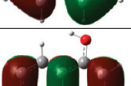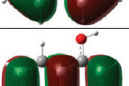
In Table 4, we present the calculated change in electron density for the *cis*- and *trans*-rotamers of 1N and 2N upon electronic excitation to the ${}^1L_b$-state. The general feature is that electronic excitation does not lead to a large change in electron density on the O-atom of the proton donating hydroxyl-group. This is in agreement with previous calculations showing that the electronic charge redistribution is only of moderate size in photoacid molecules and much larger in the conjugate photobase fueling arguments of photobase driven photoacidity.[23,25] Indeed, our quantum chemical results are consistent with previously reported values from AM1 calculations on 2N.[24] A closer inspection of the actual values shows a marked difference between 1N and 2N: for both *cis*- and *trans*-1N, electronic excitation leads to a larger transfer of the electron density from the OH-group to the naphthalene ring than in 2N.

Furthermore, the OH-group appears to exhibit a larger electron donating capability in *cis*-1N (+0.072 charge difference on the O-atom) than in the case of *trans*-1N (+0.032 on the O-atom). This can be ascribed to the $\psi_H\psi_{L+1}^*$ configuration because for this configuration, the electron density is delocalized on the OH-group in the HOMO state, while no such delocalization exists for the LUMO + 1 state (see Table 3). This charge transfer effect is reduced by contributions from the $\psi_{H-1}\psi_L^*$ configuration, where the electron is not delocalized on the OH-group in the HOMO $-$ 1 state, but instead gets delocalized onto the OH-group in the LUMO state (see Table 3).

For both *cis*- and *trans*-2N, the degree of charge transfer from the OH-group to the naphthalene ring system is smaller than that for *cis*-1N. For *cis*-2N, there is even negligible electron density change on the O-atom upon excitation. The much smaller amount of charge transfer from the OH-group to the naphthalene aromatic rings is associated with the electron distribution characteristics of the dominant electronic configurations (i.e., $\psi_H\psi_{L+1}^*$ and $\psi_{H-1}\psi_L^*$). In these $\psi_H\psi_{L+1}^*$ or $\psi_{H-1}\psi_L^*$ configurations, the electron density is delocalized between the OH-group and the aromatic ring system prior to electronic transition (ψ_H or ψ_{H-1}) and retains a larger degree of delocalization in the final state (ψ_{L+1}^* or ψ_L^*).

We can now determine the molecular dipole moment $\boldsymbol{\mu}_i^0$ and its first derivative $\boldsymbol{\mu}_i'$ and second derivative $\boldsymbol{\mu}_i''$ in the S_0- and ${}^1L_b$-states for all rotamers of 1N and 2N (see Table 5). For this, it is necessary that we consider the vectorial properties of $\boldsymbol{\mu}_i^0$, $\boldsymbol{\mu}_i$, and $\boldsymbol{\mu}_i''$. We have depicted the orientation of $\boldsymbol{\mu}_i^0$, $\boldsymbol{\mu}_i$, and $\boldsymbol{\mu}_i''$ ($i = S_0$, ${}^1L_b$) in Table 6. It follows that for *cis*-1N and *trans*-1N, the electrical dipole moment is oriented along the long-axis in both electronic states, whereas for *cis*-2N and *trans*-2N, the orientation is along the short-axis. A comparison of the orientation of our calculated electrical dipole moments and transition dipole moments with previously reported values shows a satisfying correspondence (see Table 7). *trans*-1N and both conformers of 2N are fully planar. Only *cis*-1N has a dipole moment component in the *z*-direction, i.e., orthogonal to the plane of the aromatic ring system, indicating that the O−H bond vector is pointing out-of-plane. In the S_0-state, the electrical dipole moment is larger for *cis*-1N (1.46 D) than for *trans*-1N (1.27 D), but the situation is reversed in the ${}^1L_b$-state because for *cis*-1N, a large decrease in dipole moment occurs to a value of 0.62 D, whereas for *trans*-1N, it increases to 1.91 D. An increase in the dipole moment upon electronic excitation is supported by the Lippert−Mataga analysis of the electronic absorption and emission spectra, where we find a value of $\boldsymbol{\mu}_e - \boldsymbol{\mu}_g = 0.30 \pm 0.05$ D (Figure 3). These findings can be compared to those reported in the literature: using the Gaussian 94 package at the CIS/6-31(d,p) level, it was found that 1N (no specified rotamer structure) has a dipole moment of 1.21 D in the S_0-state and 2.00 D in the ${}^1L_b$-state.[80] An even smaller change from 1.7 D in the S_0-state to 2 D in the ${}^1L_b$-state is calculated with INDO/S calculations.[81] For 2N, the *trans*-conformer has the larger electrical dipole moment in both S_0 and ${}^1L_b$-states, even though it decreases somewhat with optical excitation, whereas an increase is calculated for *cis*-2N. The calculated values for *cis*-2N are in close correspondence to those results obtained using rotationally resolved electronic Stark-effect spectroscopy.[79,82] The orientation of the first and second derivatives of the electrical dipole moment, $\boldsymbol{\mu}_i'$ and $\boldsymbol{\mu}_i''$, appears to change only slightly upon electronic excitation for *trans*-1N, *cis*-2N, and *trans*-2N but varies more for *cis*-1N. More importantly, we note that in both electronic states, $\boldsymbol{\mu}_i'$ and $\boldsymbol{\mu}_i''$ are

2781

dx.doi.org/10.1021/jp208426v |*J. Phys. Chem. A* 2012, 116, 2775–2790

Table 3. Electronic Configurations of the ^1L_a- and ^1L_b-Excited States for 1N and 2N

	naphthalene	cis-1N	trans-1N	cis-2N	trans-2N
ψ^*_{L+1} LUMO+1					
ψ^*_L LUMO					
ψ_H HOMO					
ψ_{H-1} HOMO-1					
^1L_b		-0.4051 $\psi_{H-1}\psi^*_L$ $+0.5760$ $\psi_H\psi^*_{L+1}$	-0.4061 $\psi_{H-1}\psi^*_L$ $+0.5762$ $\psi_H\psi^*_{L+1}$	0.5334 $\psi_{H-1}\psi^*_L$ -0.4282 $\psi_H\psi^*_{L+1}$ -0.1395 $\psi_H\psi^*_L$	0.5119 $\psi_{H-1}\psi^*_L$ -0.4402 $\psi_H\psi^*_{L+1}$ -0.1979 $\psi_H\psi^*_L$
^1L_a		0.6892 $\psi_H\psi^*_L$ $+0.1157$ $\psi_{H-1}\psi^*_{L+1}$	0.6881 $\psi_H\psi^*_L$ -0.1323 $\psi_{H-1}\psi^*_{L+1}$	0.6758 $\psi_H\psi^*_L$ $+0.1131$ $\psi_{H-1}\psi^*_{L+1}$ -0.1013 $\psi_H\psi^*_{L+1}$	0.6625 $\psi_H\psi^*_L$ $+0.1430$ $\psi_{H-1}\psi^*_{L+1}$ -0.1393 $\psi_H\psi^*_{L+1}$ $+0.1341$ $\psi_{H-1}\psi^*_L$

definitely not directed along the OH-bond vector. This means that despite the fact that the nature of the OH-stretching mode can be regarded to be close to that of a local mode, elongation along the OH-stretching coordinate has a larger effect on the electronic charge distribution in a direction different from the OH-bond vector.

4.2. Energy Difference between the *cis*- and *trans*-Rotamers. For gas phase 1N and 2N, the distinction between *cis*- and *trans*-rotamers has been well established.[79,82−86] Recently, it has been shown that for 2N in the S_0-state, the *cis*-rotamer is slightly more energetically favorable than the *trans*-conformer.[87,88] This order is inverted in the S_1-state, and rotational isomerization is argued to take place when 2N is excited to the ^1L_b-state. We have therefore analyzed the energetics of the *cis*- and *trans*-rotamers of 1N and 2N. Furthermore, we have calculated the gas phase energetics, and we have investigated the role of the dielectric medium on the relative energetics of these conformers. Figure 4a shows the energy difference between the *cis*- and *trans*-rotamers of 1N as a function of the dielectric function F_0. While *trans*-1N is energetically more stable than *cis*-1N in the S_0-state, the energy difference defined as $\Delta E = E_{cis} - E_{trans}$ is positive and more importantly much larger than kT at room temperature ($1kT = 0.593$ kcal/mol at 295 K). This energy difference increases with increasing F_0, which is equivalent to an increase in solvent polarity quantified by the static dielectric constant. Even though ΔE_{1N} is close to $1kT$ in the gas phase, the *trans*-rotamers are clearly favored in solution. On average, ΔE_{1N} in the range of F_0 applied in this study is equal to 0.82 kcal/mol for the ^1L_b-state

and 1.5 kcal/mol for the S_0-state. Assuming a Boltzmann distribution $\exp(-\Delta E/kT)$, the population ratio of *cis*-1N/*trans*-1N is 0.07:0.93 in the S_0-state, in accordance with a reported value obtained from an NMR study in CCl$_4$.[89] This ratio changes to 0.2:0.8 in the ^1L_b-state, provided isomer equilibration is possible. Figure 4b shows the dependence of ΔE_{2N} as a function of the dielectric function F_0 for 2N. Our results show that in the S_0-state of *cis*-2N is energetically more favorable than *trans*-2N, although the energy difference is $\sim 1kT$ for 2N in the gas phase (see Figure 4b; $F_0 = 0$). Upon electronic excitation, ΔE_{2N} decreases to $\sim 0.6kT$ for 2N in the gas phase. The energy difference diminishes when dissolving 2N in a dielectric medium, for both S_0- and ^1L_b-states, i.e., when increasing F_0. The average value of 0.53 kcal/mol found for ΔE_{2N} for 2N in solution, giving a Boltzmann distribution population ratio *cis*-2N/*trans*-2N equal to 0.71:0.29, is again in accordance with reported values from the NMR-study in CCl$_4$.[89] Upon electronic excitation, this population ratio changes to 0.63:0.37, provided equilibration takes place.

4.3. Experimental Frequency Shifts in 1N and 2N. The electronic origin absorption of the $S_0 \rightarrow {}^1L_b$ transition of gas phase 1N is located at 31 180 cm^{-1} for *cis*-1N and at 31 455 cm^{-1} for *trans*-1N.[90] A solvent-induced frequency downshift of 449 cm^{-1} occurs when dissolving 1N in *n*-hexane. This downshift increases to 455 cm^{-1} in 1,2-dichloroethane (1,2-DCE). Figure 5 shows the solvent-dependent UV/vis electronic absorption and fluorescence spectra of 1N in *n*-hexane and in 1,2-dichloroethane. The solvent-induced Stokes shift increases from 254 to 363 cm^{-1}, indicating an increase in solute−solvent interactions when going from nonpolar

2782

dx.doi.org/10.1021/jp208426v |*J. Phys. Chem. A* 2012, 116, 2775–2790

Table 4. Charge Flow Induced by the $S_0 \rightarrow {}^1L_b$ Excitation of 1N and 2N
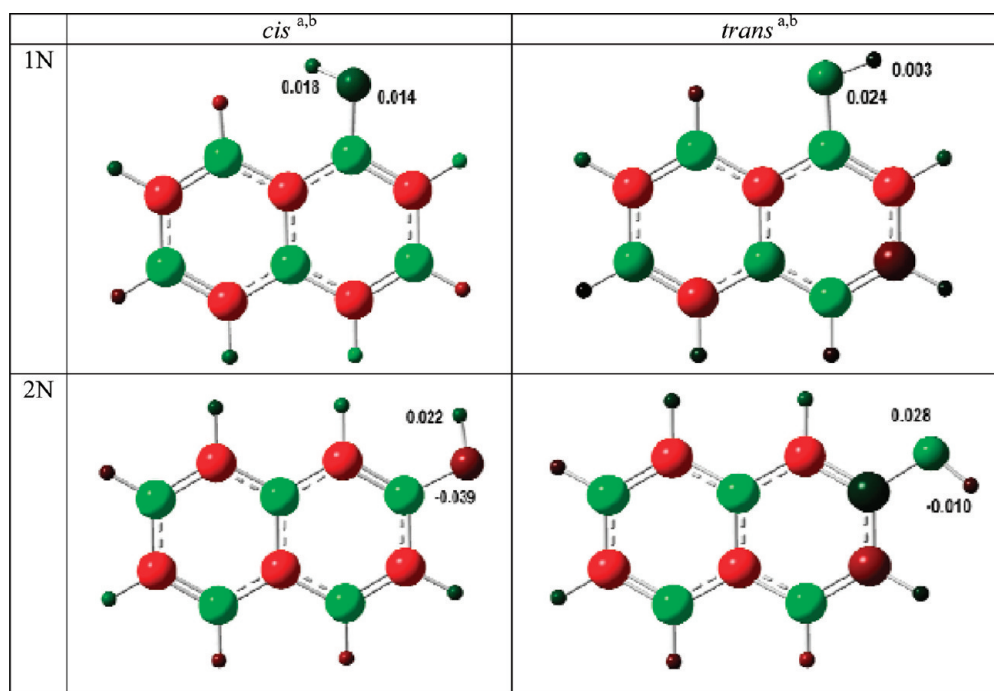
[a] The maximal negative change (i.e., increasing electron density) is represented in red, and the maximal positive change (i.e., decreasing electron density) is represented in green. [b] The ground state ESP charge was obtained by the MP2/TZVP method, while the excited state ESP charge was obtained by the TD-B3LYP/TZVP method.

Table 5. Calculated Values of μ^0, μ', and μ'' for 1N and 2N

S_0	cis-1N	trans-1N	cis-2N	trans-2N
μ^0 (D)	(1.4425, 0.1685, 0.1648)	(−1.2633, −0.1657, 0.0000)	(0.2822, −1.0500, 0.0000)	(−0.5493, 1.5094, 0.0000)
μ' (D·A^{-1}·amu$^{-1/2}$)	(−0.4823, −0.8807, −0.1090)	(−1.0552, −0.7059, 0.0000)	(−0.8472, −0.8772, 0.0000)	(−1.3049, 0.4591, 0.0000)
μ'' (D·A^{-2}·amu^{-1})	(0.6569, 2.0075, −0.1223)	(1.6293, 1.7867, 0.0000)	(2.2077, 1.4387, 0.0000)	(2.5638, −0.1233, 0.0000)

${}^1L_b$	cis-1N	trans-1N	cis-2N	trans-2N
μ^0 (D)	(0.5274, 0.2977, 0.1415)	(−1.9069, 0.1051, −0.0015)	(0.1445, −1.2190, −0.0016)	(−0.7536, 1.2544, −0.0013)
μ' (D·A^{-1}·amu$^{-1/2}$)	(−0.0187, −0.9523, −0.1074)	(−1.5174, −0.7639, 0.0000)	(−1.0066, −0.9931, 0.0000)	(−1.4784, 0.3449, 0.0002)
μ'' (D·A^{-1}·amu^{-1})	(1.0807, −2.5928, −0.3349)	(−1.8408, −2.1678, −0.0043)	(2.2640, 1.2739, 0.0000)	(2.4719, −0.1586, −0.0074)

n-hexane (ε_0 = 1.88) to weakly polar 1,2-dichloroethane (1,2-DCE; ε_0 = 10.1).

We have selected a number of alkanes and halocarbon solvents in the present study to investigate the solvent-induced vibrational frequency shifts of the OH-stretching mode in 1N and 2N. Since a significant lifetime shortening was observed in CHCl$_3$ and C$_2$Cl$_4$, and knowing that CHCl$_3$ can form weak hydrogen bonds,[33,91,92] the occurrence of specific interactions, either with the OH-group or with the aromatic π-molecular orbitals of 1N or 2N, needed to be estimated. We first investigated the steady-state IR-active fingerprint band patterns of 1N and 2N. Indeed, when specific interactions are present such as with DMSO, significant changes in both band patterns and intensities occur. However, beyond minor changes ascribable to the varying solvent polarities, the fingerprint patterns were found to be the same in all solvents used in this study for both 1N and 2N (see Figure 5). We then checked the transient IR-response of the fingerprint patterns of 1N and 2N, which were also found to be similar in

frequency positions and band cross-sections for all solvents used in this study. Although in 2N no dynamics were observed up until 50 ps, in 1N, significant quenching in CHCl$_3$ and C$_2$Cl$_4$ already occurs on these time scales. We therefore measured the dynamics of the OH-stretching mode in CHCl$_3$ to see if the vibration was affected by a possible exciplex formation. As shown in Figure 5, this is not the case: quenching and subsequent partial bleach recovery is observed, but this affects neither the frequency nor the band shape of the vibration. We performed one last test in order to confirm that the quenching mechanism does not involve any direct interaction with the OH-bond. For this, the transient fingerprint region of 1N complexed with dimethylsulfoxide (DMSO) in C$_2$Cl$_4$ was measured. In such a system, given the very high complexation constant of DMSO and 1N through the formation of a medium strong HB, no direct interaction of the OH-group with nonpolar C$_2$Cl$_4$ can occur: the OH bond is effectively tied-up. As the same quenching behavior was observed, we conclude that the quenching interaction with the
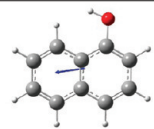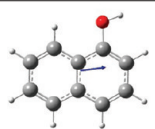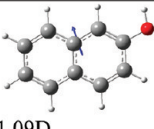
Table 6. Orientation of μ^0, μ', and μ'' in 1N and 2N
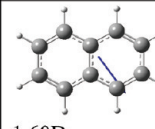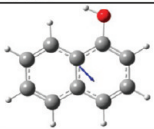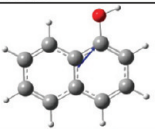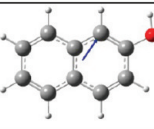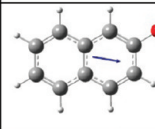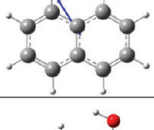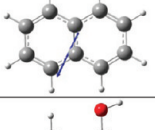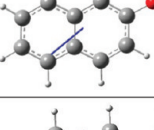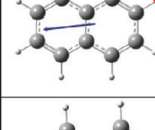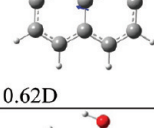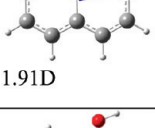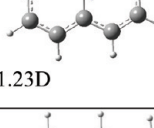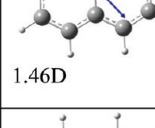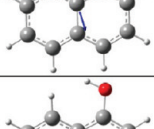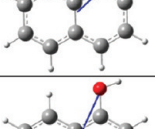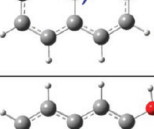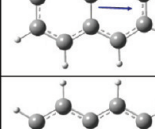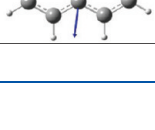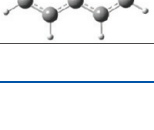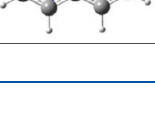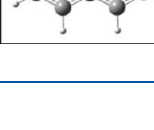
	cis-1N	*trans*-1N	*cis*-2N	*trans*-2N
S_0, μ	1.46D	1.27D	1.09D	1.60D
S_0, μ'				
S_0, μ''				
^1L_b, μ	0.62D	1.91D	1.23D	1.46D
^1L_b, μ'				
^1L_b, μ''				

Table 7. Calculated Angles (Absolute Values, with a Range of 0–90°) of Transition Dipole and Electrical Dipole Moments Relative to the *x*-Axis (Along the Long-Axis)

	calcd angle of transition dipole moment (deg)	exptl angle of transition dipole moment (deg)[a]	calculated angle of electrical dipole moment (deg)		experimental angle of electrical dipole moment (deg)[b]	
			S_0	^1L_b	S_0	^1L_b
cis-1N	11	6	9	32		
trans-1N	18	33	7	3		
cis-2N	49	66	75	83	70	82
trans-2N	61	74	70	59		

[a] From ref 79. [b] From ref 82.

halocarbon solvents occurs with the aromatic system. This result is further supported by the fact that quenching is also observed in the parent naphthalene molecule, which does not have any OH bond.[53,54]

Figure 6a shows the steady-state IR spectra of 1N depicting the solvent-dependent OH-stretching transition. In a fashion similar to that of 2N,[49] a larger frequency downshift and concomitant line broadening are observed when going from nonpolar *n*-hexane to polar 1,2-DCE. When plotting the experimental line width as a function of frequency position (Figure 6c), a linear correlation results that can even be extrapolated to the known value for gas phase 1N.[83] The transient IR spectra measured at 10 ps show

ground state bleach signals and positive absorbance changes at lower frequency values than the OH-stretching frequency of 1N in the S_0-state (Figure 6b). A decrease of the OH-stretching frequency thus occurs upon electronic excitation of 1N, in a fashion similar to that observed for 2N.[49]

A line shape fitting routine was applied to determine the solvent-dependent frequency shift and line width of the OH-stretching mode of 1N in the ^1L_b-state. As for the electronic ground state, an empirical frequency–line width correlation is obtained for the OH-stretching mode of 1N in the electronically excited state (Figure 6c). In contrast to 2N, however, no value for gas phase 1N in the ^1L_b-state has been reported in the literature.
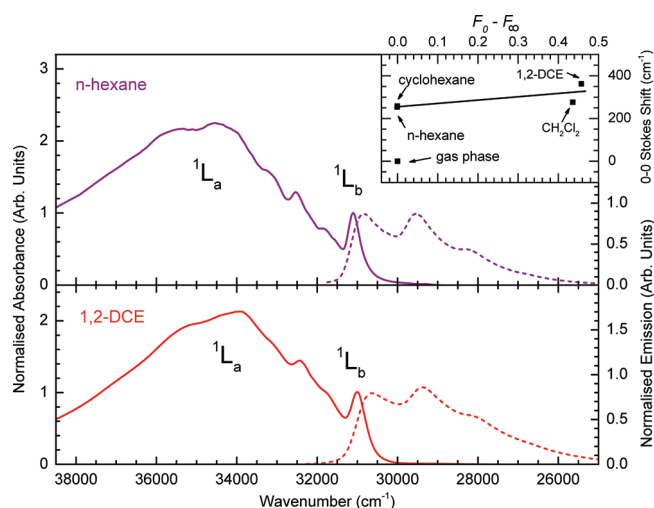
2784

dx.doi.org/10.1021/jp208426v |*J. Phys. Chem. A* 2012, 116, 2775–2790

Figure 3. UV/vis absorption and emission spectra of 1N in *n*-hexane and 1,2-dichloroethane (1,2-DCE). The upper right inset shows the Lippert—Mataga plot of the 0—0 Stokes shift between the electronic absorption and emission origin transitions as a function of $F_0 - F_\infty = (2\varepsilon_0 - 2)/(2\varepsilon_0 + 1) - (2\varepsilon_\infty - 2)/(2\varepsilon_\infty + 1)$ from which $\Delta\boldsymbol{\mu}^0 = \boldsymbol{\mu}_e^0 - \boldsymbol{\mu}_g^0 = 0.30 \pm 0.05$ D can be derived.

Figure 4. Energy difference between the *cis*- and *trans*-rotamers of 1N (a) and between the *cis*- and *trans*-rotamers of 2N (b).

Because the linear frequency position—line width correlation occurs for 2N in both electronic ground and excited states,[49] we argue that we can expect this to also be the case for 1N. We can therefore extrapolate our experimental data to predict the OH-stretching frequency of gas phase 1N in the ${}^1L_b$-state to be equal to 3620 ± 10 cm^{-1}. Figure 7 shows the experimentally measured OH-stretching frequency shifts as a function of F_0, for 1N and 2N, in the S_0 and ${}^1L_b$ states. Even though the intercept turns out to be too small for both 1N and 2N and thus cannot accurately be determined with our current data set, we can derive the ratio of the slope values S_e/S_g by a linear fit to be equal to 1.13 ± 0.05 for 1N and 1.23 ± 0.05 for 2N.

5. DISCUSSION

5.1. Calculated Molecular Parameters. According to eq 14a, the slope of the frequency shifts vs F_0 is governed by the following molecular parameters: the electrical dipole moment $(\boldsymbol{\mu}_i^0)$, the electrical dipole first $(\boldsymbol{\mu}_i')$ and second $(\boldsymbol{\mu}_i'')$ derivatives, the ratio of cubic to quadratic force constants (V'''/V''), the harmonic vibrational frequency (ν_0), the vibrational reduced mass (m), and the Onsager cavity radius (a_i). We have listed the relevant product terms in Table 8. It turns out that for both conformers of 1N and 2N in both electronic states the $-(V_e''')/(V_e'')\boldsymbol{\mu}_e'\cdot\boldsymbol{\mu}_e^0$ term dominates the predicted solvent-induced vibrational frequency shift. While for *trans*-1N, *cis*-2N, and *trans*-2N the $\boldsymbol{\mu}_i'\cdot\boldsymbol{\mu}_i^0$ term has positive values, it is negative for *cis*-1N. As a result, the calculated slope S_i is negative for *cis*-1N, i.e., the solute—solvent interaction leads to a OH-stretching frequency upshift for this conformer. The positive slope S_i for *trans*-1N, *cis*-2N, and *trans*-2N implies instead a frequency downshift for the OH-stretching mode upon embedding the solute in a dielectric medium. In all cases, we observe a larger absolute value for the slope S_i in the ${}^1L_b$-state than in the S_0-state. The intercept B_i is calculated to be on the order of a few wavenumbers for both *cis*- and *trans*-conformers of 1N and 2N in the S_0-state. Electronic excitation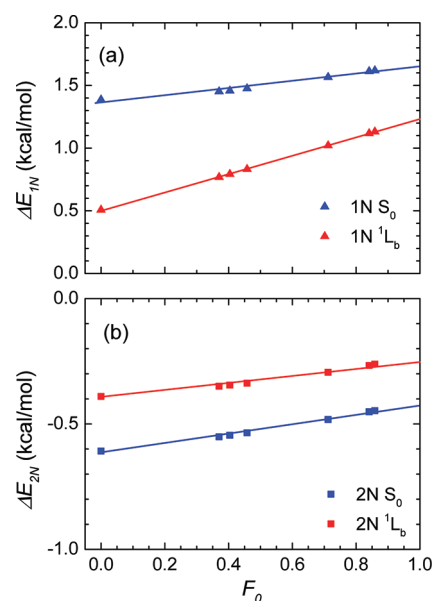 of the 2N conformers does not change the value of the intercept significantly. Only for *cis*- and *trans*-1N in the ${}^1L_b$-state is the intercept calculated to increase to $\sim$14—15 cm^{-1}. Finally, whereas the ratio of slopes (S_e/S_g) appears to be similar for *cis*-2N (1.41) and *trans*-2N (1.42), for *trans*-1N (1.61), it has a much smaller value than that for *cis*-1N (2.71).

The Pullin—van der Zwan—Hynes approach also enables us to explain why we only have observed a small time-dependent solvent-induced vibrational frequency shift in the case of the most polar solvent used, i.e., for 2N in 1,2-DCE.[49] Use of eq 24 with the parameter values given in Tables 5 and 8 provides insight into this. It follows that for alkane solvents like *n*-hexane and cyclohexane the ratio between the time-dependent shift and overall shift for the OH-stretching mode of 1N or 2N are close to zero, because $F_0 - F_\infty = F_{or} \approx 0$. This factor becomes significant for polar solvents, such as 1,2-DCE (see Figure 1b). Averaging over the *cis*- and *trans*-rotamers of 2N, we estimate a maximum theoretical value of 15%. The lower experimental value of 5% may be due to the limited temporal resolution of 0.2 ps in the experiments, which may have caused us to miss the earliest time-dependent response.[49] More importantly, for 1N this value is expected to be 2—3 times smaller than that for 2N and will thus be below the spectral resolution of our equipment. In addition, one can also predict that this ratio will be at most 20% even in solvents of higher polarity such as DMSO. However, this is solely an academic discussion, as in this case, hydrogen bonding will lead to a change of all the parameters.

5.2. Comparison between Experiment and Theory. A good agreement between theory and experiment is found for the solvent-dependent OH-stretching frequency shifts as a function of F_0 when the perturbative approach of Pullin is parametrized at the TD-DFT level of theory. As the predicted values for the intercept are smaller than the uncertainty in the linear fits in Figure 7, we focus our analysis on the slopes of the curves. To properly compare theory and experiments at room temperature, we perform a proper ensemble average over possible conformers. We not only consider the population ratio of the *cis*- and *trans*-conformers but also estimate a minimal exchange rate between the
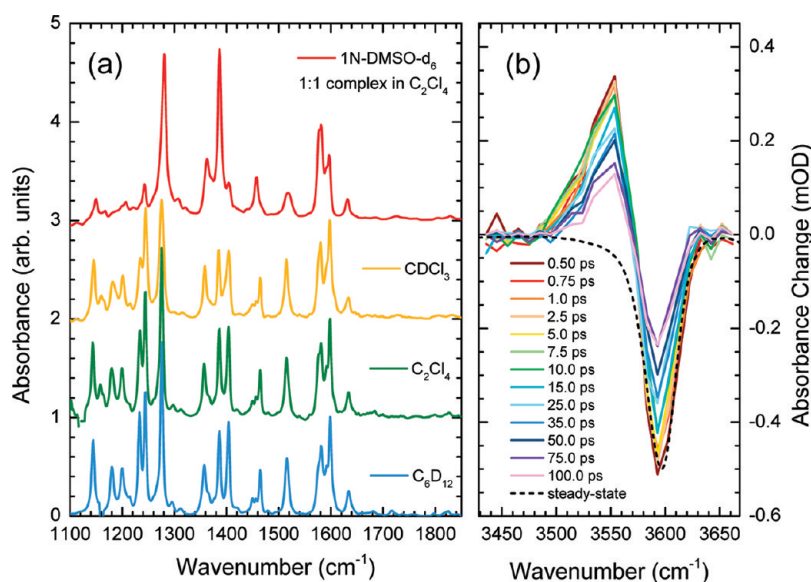
Figure 5. (a) Steady-state FT-IR spectra of 1N in different solvents, showing that only a specific hydrogen bond in a 1:1 complex of 1N with DMSO-d_6 (dissolved in C_2Cl_4) significantly affects the fingerprint pattern; (b) Transient IR-spectrum of 1N in CDCl$_3$ showing the time-dependent dynamics of the OH-stretching mode.
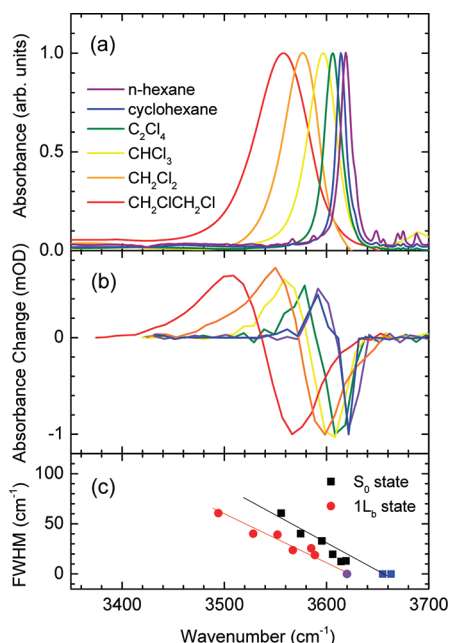

Figure 6. (a) Steady-state IR spectra of 1N; (b) transient IR spectra of 1N measured at a 10 ps pulse delay; (c) correlation between the solvent-dependent frequency shift and transition bandwidth of 1N in the S_0 (black squares) and ^1L_b (red dots) electronic states, including reported gas phase values for 1N in the S_0-state (blue squares) and the extrapolated value in the ^1L_b-state for gas phase 1N (purple dot).

two conformers. For 2N in the S_0-state, it has been reported that the OH-stretching frequency is located at 3652 cm^{-1} [85,88] or 3654 cm^{-1} [84,93] for *cis*-2N and at 3661 cm^{-1} for *trans*-2N. [84,93] The value for 2N in the electronic excited ^1L_b-state (3609 cm^{-1}) refers to *cis*-2N, although, it has been argued that *cis* → *trans* isomerization occurs. [88] For 1N in the S_0-state, values of 3661 cm^{-1} for the *cis*-1N conformer and 3655 cm^{-1} for the

trans-1N conformer have been reported. [83] As a result, the *cis*- and *trans*-conformers can only be distinguished if spectral features can be recorded with a resolution better than the frequency spacing of the OH-stretching resonances of the *cis*- and *trans*-conformers, i.e., 6−8 cm^{-1}.

In the experimental spectra of 1N and 2N in solution, only one spectrally broadened OH-stretching band is found, both in the S_0 and the ^1L_b-states. Setting aside a limited spectral resolution for the transient IR measurements and knowing that for the most polar solvent used in this study (1,2-DCE) the line broadening is more than 1 order of magnitude larger than the OH-stretching frequency spacing of the *cis*- and *trans*-conformers, one should, in principle, be able to monitor the two conformers in *n*-hexane or cyclohexane with the steady-state FT-IR spectrometer where the spectral line width is 13 cm^{-1} (fwhm). However, as the line shapes of the OH-stretching bands of 1N and 2N are close to fully Lorentzian, one can conclude that the exchange between the two conformers is ultrafast. A coalescence of the OH-stretching bands of the two rotamers can be calculated to occur for exchange times shorter than 2.5 ps. For 2N, the calculated value for the slope ratio is almost equal for both conformers. Our experimental value is about 13% less than the calculated value. Whereas for 2N, we have an ensemble average of about equal amounts of *cis*- and *trans*-conformers in solution, this is certainly not the case for 1N, where in the S_0-state the *trans*-conformer dominates. The average population ratio between *cis*-1N and *trans*-1N is 0.20:0.80 in the ^1L_b-state and 0.07:0.93 in the S_0-state (section 4.2). Thus, the slope for 1N after correction using the Boltzmann distribution of the *cis*- and *trans*-rotamers is 1.12. This is remarkably close to the experimentally found value of 1.13.

The solvatochromic vibrational frequency shift upon excitation is observed to be different between 1N and 2N. From Figure 7, we see that, in a particular solvent medium, the frequency shift ω_{ge} upon excitation (i.e., $S_0 \rightarrow {}^1L_b$-transition) of 1N is smaller than that of 2N. According to eq 14,

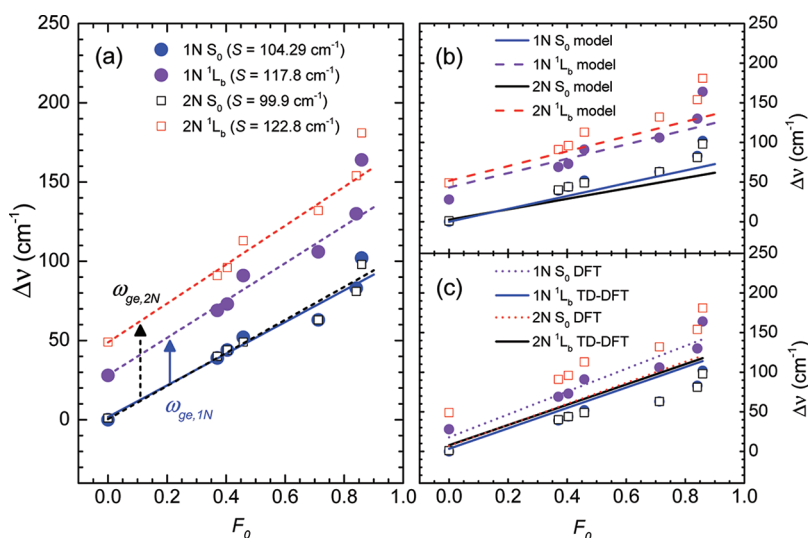$$V_0^g - V_s^g = S_g F_0 + B_g \qquad (25a)$$

Figure 7. Experimental frequency shifts for the S_0- and ^1L_b-states of 1N (dots) and 2N (squares), relative to the frequency of the S_0-state of 1N (3658 cm^{-1}), together with solid and dashed lines obtained by (a) experimental fits, (b) predictions according to Pullin's model with factors calculated with TD-DFT calculations, and (c) predictions according to the PCM model in Gaussian 09 at the TD-DFT level with the PCM solvent.

Table 8. Calculated Parameter Values for 1N and 2N Governing the Solvent-Induced Vibrational Frequency Shifts

term	cis-1N ^1L_b	cis-1N S_0	trans-1N ^1L_b	trans-1N S_0	cis-2N ^1L_b	cis-2N S_0	trans-2N ^1L_b	trans-2N S_0
$\boldsymbol{\mu}_i'' \cdot \boldsymbol{\mu}_i^0$ (D^2 A^{-2} amu^{-1})	-0.2493	0.5892	3.2824	-2.3544	-1.2257	-0.8876	-2.0618	-1.5944
$\boldsymbol{\mu}_i' \cdot \boldsymbol{\mu}_i^0$ (D^2 A^{-1} amu$^{-1/2}$)	-0.3085	-0.8621	2.8132	1.4500	1.0651	0.6820	1.5468	1.4097
V_i'''/V_i'' (A^{-1} amu$^{-1/2}$)	-7.1204	-7.1510	-7.0932	-7.0928	-7.1234	-7.1660	-7.1295	-7.1714
$\boldsymbol{\mu}_i'' \cdot \boldsymbol{\mu}_i^0 - (V_i''')/(V_i'')\boldsymbol{\mu}_i' \cdot \boldsymbol{\mu}_i^0$	-2.4471	-5.9156	23.2370	7.9302	6.3614	3.9996	8.9661	8.5151
$[\boldsymbol{\mu}_e'' - (V_e''/V_e')\boldsymbol{\mu}_e'] \cdot [\boldsymbol{\mu}_g^0 - \boldsymbol{\mu}_e^0]$	0.5798		4.8622		2.7099		1.9909	
a_i (Å)	0.7611	1.4195	1.5524	1.2667	1.1762	1.1260	1.3071	1.4374
v_0^i (cm^{-1})	3620	3661	3620	3655	3609	3653	3609	3661
S_i (cm^{-1})^a	-129.96	-47.883	145.43	90.48	91.82	65.00	94.29	66.38
$\boldsymbol{\mu}_i' \cdot \boldsymbol{\mu}_i'$ (D^2 A^{-2} amu^{-1})	0.9188	1.0201	2.8860	1.6117	1.9995	1.4872	2.3046	1.9135
$\boldsymbol{\mu}_i' \cdot \boldsymbol{\mu}_i' + \boldsymbol{\mu}_i^0 \cdot \boldsymbol{\mu}_i''$	0.6695	1.6093	6.1684	-0.7427	0.7738	0.5996	0.2428	0.3191
B_i (cm^{-1})^b	14.2223	5.2105	15.4421	-0.3896	4.4674	3.8981	1.0214	0.9951
S_e/S_g	2.71		1.61		1.41		1.42	

$^a S_i = (1/8\pi^2 m v_0^i a_i^3)(\boldsymbol{\mu}_i' \cdot \boldsymbol{\mu}_i'' - (V_i''')/(V_i'')\boldsymbol{\mu}_i^0 \cdot \boldsymbol{\mu}_i')$. $^b B_i = (F_\infty/8\pi^2 m v_0^i a_i^3)(\boldsymbol{\mu}_i' \cdot \boldsymbol{\mu}_i' + \boldsymbol{\mu}_i^0 \cdot \boldsymbol{\mu}_i'')$ is the intercept, where $F_\infty \approx 0.4$.

$$V_0^e - V_s^e = S_e F_0 + B_e \qquad (25b)$$

from which we derive

$$\omega_{ge} = V_s^g - V_s^e$$
$$= (V_0^g - V_0^e) + (S_e - S_g)F_0 + (B_e - B_g) \qquad (25c)$$

Hence, ω_{ge} is determined by the frequency shift upon excitation in the gas phase ($v_0^g - v_0^e$), the slope difference ($S_e - S_g$), and the intercept difference ($B_e - B_g$) of the frequency shifts between electronic excited and ground states upon solvation. Here, one can compare our findings using the OH-stretching mode as a local solvation probe with those obtained with UV/vis electronic spectroscopy,[30,36,80] where the photoacid−solvent interaction is governed by the full solvation shell interacting with the electronic charge distribution of the chromophore. In these UV/vis electronic spectroscopic studies, the semiempirical Kamlet−Taft analysis was performed on a larger set of solvents, including

those with specific hydrogen bonding interactions. It was found that for 2N the nonspecific solute−solvent interactions (as described by the coefficient for the solvent polarity/polarizability parameter π^*) are smaller than those of 1N, and accordingly for 2N, smaller contributions to electronic transition frequency shifts result through this component. This, however, is not what we observe when we inspect the electronic Stokes shift of 2N and 1N in our set of nonpolar/weakly polar solvents. In contrast, we find that the magnitude of the solvent-induced electronic Stokes shift is fully consistent with the magnitude of the solvent-induced OH-stretching frequency shift, namely, being smaller for 1N than for 2N. Whereas the magnitude of the electronic Stokes shift as a function of $(F_0 - F_\infty)$ scales with $(\boldsymbol{\mu}_e - \boldsymbol{\mu}_g)^2$, as, e.g., defined by the Lippert−Mataga equation,[39,58,94] the difference in solvent-induced OH-stretching frequency shifts in electronic excited and electronic ground state follows eq 25c with which we can explain the smaller solvent-induced effects on the OH-stretching mode of 1N than those of 2N. This is a consequence of a smaller value for the gas phase frequency shift ($v_0^g - v_0^e$) for 1N compared to

Table 9. Calculated and Experimental OH-Stretch Vibrational Frequencies

	calcd frequency $(cm^{-1})^a$	scaled frequency $(cm^{-1})^b$	calcd ω_{ge} (cm^{-1}) for $S_0 \rightarrow {}^1L_b$ transition	exptl frequency $(cm^{-1})^c$	exptl ω_{ge} (cm^{-1}) for $S_0 \rightarrow {}^1L_b$ transition^c
cis-1N, S_0	3850.6	3659	56	3661	38^d
cis-1N, ${}^1L_b$	3791.5	3603		3620^d	
trans-1N, S_0	3841.6	3650	37	3655	
trans-1N, ${}^1L_b$	3802.0	3613		3620^d	
cis-2N, S_0	3840.4	3649	25	3653	48^d
cis-2N, ${}^1L_b$	3813.9	3624		3609^d	
trans-2N, S_0	3852.7	3661	32	3661	
trans-2N, ${}^1L_b$	3818.8	3629		3609^d	

^{a} The S_0-state was calculated using the MP2/TZVP method; the ${}^1L_b$-state was calculated with the TD-B3LYP/TZVP method. ^{b} Scaling factor: 0.9502. ^{c} Experimental values of 1N and 2N in the gas phase were taken from refs 83−85 and 93. ^{d} Average value for cis- and trans-conformers.

that of 2N and values with opposite signs for the slope difference $(S_e - S_g)$ for cis-1N and trans-1N, whereas $(S_e - S_g)$ has a positive value for both cis-2N and trans-2N.

For the comparison between the OH-stretching frequency shifts of 1N and 2N upon electronic excitation, the gas phase factor $(v_0^g - v_0^e)$ also plays a key role in dictating the frequency shifts observed in solution. Frequency shifts upon electronic excitation in the gas phase are caused by the charge rearrangement in 1N and 2N. Hence, in the following, we explore the electrostatic potential (ESP) charge difference due to the $S_0 \rightarrow {}^1L_b$-transition for 1N and 2N, for both the cis- and trans-rotamers. For the calculation of the ESP charge, the MP2/TZVP method was used for electronic ground states, and the TD-B3LYP/TZVP method was used for electronic excited states. The rationalization for choosing the ab initio methods was based on the fact that the calculated OH-stretching vibrational frequencies using these methods for the ground and excited states of 1N and 2N show good consistency with the experimental vibrational frequencies (see Table 9).

The comparison of experimental vibrational frequency shifts and the corresponding shifts computed with Pullin's model shows improvement over predictions based on the standard PCM techniques as implemented in Gaussian 09 at the same level of TD-DFT theory. This is quite remarkable, considering the simplicity of Pullin's model of dynamical solvatochromic effects. When compared to more standard techniques, Pullin's model has the disadvantage of simplifying the electrostatic description of the molecule to a point dipole. However, the reaction field in the polarizable continuum includes both static and optical response functions induced by changes in the molecular point dipole moment associated with vibrations and/or electronic excitations. It is therefore natural to conclude that the description of solvatochromic effects based on standard PCM models would benefit from extensions of the methods to include the optical response of the solvent due to vibronic or electronic excitations.

6. CONCLUSIONS

We have combined ultrafast UV/mid-infrared pump−probe spectroscopy and theoretical modeling of solvatochromic effects to investigate the OH-stretching mode of 1-naphthol (1N) and 2-naphthol (2N) in the ground (S_0) and first excited $({}^1L_b)$ states in several solvents of moderate polarity, where specific interactions such as hydrogen bonding are absent. To understand the observed solvent-induced

vibrational frequency shifts in both electronic states, we have applied the perturbative treatment of Pullin, as refined with the van der Zwan−Hynes relationship to incorporate the time-dependent response of solvent shells upon the electronic excitation of the solute. To quantify the different contributions in this perturbative approach, we have performed quantum chemical TD-DFT calculations to determine the role of the electronic charge distributions in the S_0- and ${}^1L_b$-states of 1N, as reflected by the molecular electrical dipole moment and its first and second derivatives along the OH-stretching coordinate, as well as the degree of anharmonicity of the molecular vibration.

Further refinements of the approach may include the incorporation of solute polarizability, as well as extension to cases where specific interactions are present. The influence of solute polarizability on solvent-induced vibrational frequency shifts can easily be estimated, provided information on molecular polarizability in a particular electronic state is available. According to Pullin,[43,44] one should then replace the respective f with $f/(1 - f\alpha)$ present in the different terms in the expressions for the solvent-induced vibrational frequency shifts. A solute polarizability α leads to an increase of solute−solvent interactions for the polar solvents, with concomitant large vibrational frequency shifts. Using available polarizability data on the parent naphthalene molecule[95,96] and assuming similar values for the polarizability for 1N and 2N in both S_0- and ${}^1L_b$-states as those of naphthalene, suggests a 10−20% additional frequency shift for the most polar solvent used in this study.

A natural choice to explore the potential applicability of the approach demonstrated here will be to investigate the solvent-induced frequency shifts of OH-stretching modes of photoacid−base complexes. While the perturbative approach of the solute−solvent interactions may be sufficient for hydrogen-bonded OH-groups as well, the impact of diagonal and off-diagonal anharmonicities is expected to be more pronounced. Exploring this aspect of Pullin's perturbative approach will be an intriguing topic as the next testing ground for understanding solvent-induced vibrational frequency shifts in hydrogen-bonded photoacid−base complexes.

■ AUTHOR INFORMATION

Corresponding Author

*E-mail: nibberin@mbi-berlin.de (E.T.J.N.); victor.batista@yale.edu (V.S.B.).

■ REFERENCES

(1) Weller, A. *Prog. React. Kinet. Mech.* **1961**, *1*, 187.

(2) Vander Donckt, E. *Prog. React. Kinet. Mech.* **1970**, *5*, 273.

(3) Ireland, J. F.; Wyatt, P. A. H. *Adv. Phys. Org. Chem.* **1976**, *12*, 131.

(4) (a) Martynov, I. Y.; Demyashkevich, A. B.; Uzhinov, B. M.; Kuz'min, M. G. *Usp. Khim.* **1977**, *46*, 3. (b) *Russ. Chem. Rev.* **1977**, *46*, 1.

(5) Arnaut, L. G.; Formosinho, S. J. *J. Photochem. Photobiol., A* **1993**, *75*, 1.

(6) Tolbert, L. M.; Solntsev, K. M. *Acc. Chem. Res.* **2002**, *35*, 19.

(7) Barroso, M.; Arnaut, L. G.; Formosinho, S. J. *J. Photochem. Photobiol., A* **2002**, *154*, 13.

(8) Pines, E. UV-Visible Spectra and Photoacidity of Phenols, Naphthols and Pyrenols. In *Chemistry of Phenols*; Rappoport, Z., Ed.; Wiley: New York, 2003; p 491.

(9) Kosower, E. M.; Huppert, D. *Annu. Rev. Phys. Chem.* **1986**, *37*, 127.

(10) Pines, E.; Pines, D. Proton Dissociation and Solute–Solvent Interactions Following Electronic Excitation of Photoacids. In *Ultrafast Hydrogen Bonding Dynamics and Proton Transfer Processes in the Condensed Phase*; Elsaesser, T., Bakker, H. J., Eds.; Kluwer Academic Publishers: Dordrecht, The Netherlands, 2002; p 155.

(11) Agmon, N. *J. Phys. Chem. A* **2005**, *109*, 13.

(12) Cheshnovsky, O.; Leutwyler, S. *J. Chem. Phys.* **1988**, *88*, 4127.

(13) Knochenmuss, R.; Leutwyler, S. *J. Chem. Phys.* **1989**, *91*, 1268.

(14) Breen, J. J.; Peng, L. W.; Willberg, D. M.; Heikal, A.; Cong, P.; Zewail, A. H. *J. Chem. Phys.* **1990**, *92*, 805.

(15) Plusquellic, D. F.; Tan, X.-Q.; Pratt, D. W. *J. Chem. Phys.* **1992**, *96*, 8026.

(16) Syage, J. *J. Phys. Chem.* **1995**, *99*, 5772.

(17) Knochenmuss, R.; Fischer, I. *Int. J. Mass Spectrom.* **2002**, *220*, 343.

(18) David, O.; Dedonder-Lardeux, C.; Jouvet, C. *Int. Rev. Phys. Chem.* **2002**, *21*, 499.

(19) Tanner, C.; Manca, C.; Leutwyler, S. *Science* **2003**, *302*, 1736.

(20) Domcke, W.; Sobolewski, A. L. *Science* **2003**, *302*, 1693.

(21) Pines, D.; Pines, E. Solvent Assisted Photoacidity. In *Hydrogen-Transfer Reactions*; Hynes, J. T., Klinman, J. P., Limbach, H.-H., Schowen, R. L., Eds.; Wiley-VCH: Weinheim, Germany, 2007; Vol. 1: Physical and Chemical Aspects I–III, p 377.

(22) Melnichuk, A.; Bartlett, R. J. *J. Chem. Phys.* **2011**, *134*, 244303.

(23) Granucci, G.; Hynes, J. T.; Millié, P.; Tran-Thi, T.-H. *J. Am. Chem. Soc.* **2000**, *122*, 12243.

(24) Agmon, N.; Rettig, W.; Groth, C. *J. Am. Chem. Soc.* **2002**, *124*, 1089.

(25) Hynes, J. T.; Tran-Thi, T. H.; Granucci, G. *J. Photochem. Photobiol., A* **2002**, *154*, 3.

(26) Barbara, P. F.; Jarzeba, W. *Adv. Photochem.* **1990**, *15*, 1.

(27) Castner, E. W., Jr.; Maroncelli, M. *J. Mol. Liq.* **1998**, *77*, 1.

(28) Bagchi, B.; Jana, B. *Chem. Soc. Rev.* **2010**, *39*, 1936.

(29) Solntsev, K. M.; Huppert, D.; Tolbert, L. M.; Agmon, N. *J. Am. Chem. Soc.* **1998**, *120*, 7981.

(30) Solntsev, K. M.; Huppert, D.; Agmon, N. *J. Phys. Chem. A* **1998**, *102*, 9599.

(31) Barrash-Shiftan, N.; Brauer, B. B.; Pines, E. *J. Phys. Org. Chem.* **1998**, *11*, 743.

(32) Pines, E.; Pines, D.; Ma, Y.-Z.; Fleming, G. R. *ChemPhysChem* **2004**, *5*, 1315.

(33) Chudoba, C.; Nibbering, E. T. J.; Elsaesser, T. *Phys. Rev. Lett.* **1998**, *81*, 3010.

(34) Nibbering, E. T. J.; Chudoba, C.; Elsaesser, T. *Isr. J. Chem.* **1999**, *39*, 333.

(35) Asbury, J. B.; Wang, Y. Q.; Lian, T.-Q. *Bull. Chem. Soc. Jpn.* **2002**, *75*, 973.

(36) Magnes, B.-Z.; Pines, D.; Strashnikova, N.; Pines, E. *Solid State Ionics* **2004**, *168*, 225.

(37) Baba, H. *Bull. Chem. Soc. Jpn.* **1961**, *34*, 82.

(38) Nishimoto, K. *J. Phys. Chem.* **1963**, *67*, 1443.

(39) Mataga, N.; Kubota, T. *Molecular Interactions and Electronic Spectra*; Marcel Dekker: New York, 1970.

(40) Buckingham, A. D. *Proc. R. Soc. London Ser., A* **1958**, *248*, 169.

(41) Buckingham, A. D. *Proc. R. Soc. London Ser., A* **1960**, *255*, 32.

(42) Buckingham, A. D. *Trans. Faraday Soc.* **1960**, *56*, 753.

(43) Pullin, A. D. E. *Spectrochim. Acta* **1958**, *13*, 125.

(44) Pullin, A. D. E. *Proc. R. Soc. London Ser., A* **1960**, *255*, 39.

(45) Herrebout, W. A.; Delanoye, S. N.; van der Veken, B. J. *J. Phys. Chem. A* **2004**, *108*, 6059.

(46) McDowell, S. A. C.; Buckingham, A. D. *J. Am. Chem. Soc.* **2005**, *127*, 15515.

(47) McDowell, S. A. C.; Buckingham, A. D. *Spectrochim. Acta, Part A* **2005**, *61*, 1603.

(48) van der Zwan, G.; Hynes, J. T. *J. Phys. Chem.* **1985**, *89*, 4181.

(49) Prémont-Schwarz, M.; Xiao, D.; Batista, V. S.; Nibbering, E. T. J. *J. Phys. Chem. A* **2011**, *115*, 10511.

(50) Frisch, M. J.; Trucks, G. W.; Schlegel, H. B.; Scuseria, G. E.; Robb, M. A.; Cheeseman, J. R.; Scalmani, G.; Barone, V.; Mennucci, B.; Petersson, G. A.; Nakatsuji, H.; Caricato, M.; Li, X.; Hratchian, H. P.; Izmaylov, A. F.; Bloino, J.; Zheng, G.; Sonnenberg, J. L.; Hada, M.; Ehara, M.; Toyota, K.; Fukuda, R.; Hasegawa, J.; Ishida, M.; Nakajima, T.; Honda, Y.; Kitao, O.; Nakai, H.; Vreven, T.; Montgomery, J. A., Jr.; Peralta, J. E.; Ogliaro, F.; Bearpark, M.; Heyd, J. J.; Brothers, E.; Kudin, K. N.; Staroverov, V. N.; Kobayashi, R.; Normand, J.; Raghavachari, K.; Rendell, A.; Burant, J. C.; Iyengar, S. S.; Tomasi, J.; Cossi, M.; Rega, N.; Millam, J. M.; Klene, M.; Knox, J. E.; Cross, J. B.; Bakken, V.; Adamo, C.; Jaramillo, J.; Gomperts, R.; Stratmann, R. E.; Yazyev, O.; Austin, A. J.; Cammi, R.; Pomelli, C.; Ochterski, J. W.; Martin, R. L.; Morokuma, K.; Zakrzewski, V. G.; Voth, G. A.; Salvador, P.; Dannenberg, J. J.; Dapprich, S.; Daniels, A. D.; Farkas, O.; Foresman, J. B.; Ortiz, J. V.; Cioslowski, J.; Fox, D. J. *Gaussian 09*, revision A.1; Gaussian, Inc.: Wallingford, CT, 2009.

(51) Platt, J. R. *J. Chem. Phys.* **1949**, *17*, 484.

(52) Grimme, S.; Parac, M. *ChemPhysChem* **2003**, *3*, 292.

(53) Behera, P. K.; Mukherjee, T.; Mishra, A. K. *J. Lumin.* **1995**, *65*, 137.

(54) Sujatha, J.; Mishra, A. K. *J. Lumin.* **1997**, *65*, 137.

(55) Adamczyk, K.; Premont-Schwarz, M.; Pines, D.; Pines, E.; Nibbering, E. T. J. *Science* **2009**, *326*, 1690.

(56) Yu, H. *J. Environ. Sci. Health, Part C* **2002**, *20*, 149.

(57) Brahmia, O.; Richard, C. *Photochem. Photobiol. Sci.* **2005**, *4*, 454.

(58) Reichardt, C. *Solvents and Solvent Effects in Organic Chemistry*; Wiley-VCH: Weinheim, Germany, 2003.

(59) Kirkwood, J. G. is acknowledged in West, W.; Edwards, R. T. *J. Chem. Phys.* **1937**, *5*, 14.

(60) Bauer, E.; Magat, M. *J. Phys. Radium* **1938**, *9*, 319.

(61) Bekárek, V.; Mikulecká, A. *Collect. Czech. Chem. Commun.* **1978**, *43*, 2879.

(62) Kolling, O. W. *J. Phys. Chem.* **1996**, *100*, 16087.

(63) (a) Lutskii, A. E.; Prezhdo, V. V.; Degtereva, L. I.; Gordienko, V. G. *Usp. Khim.* **1982**, *51*, 1398. (b) *Russ. Chem. Rev.* **1982**, *51*, 802.

(64) Nibbering, E. T. J.; Elsaesser, T. *Chem. Rev.* **2004**, *104*, 1887.

(65) Heyne, K.; Huse, N.; Dreyer, J.; Nibbering, E. T. J.; Elsaesser, T.; Mukamel, S. *J. Chem. Phys.* **2004**, *121*, 902.

(66) Dreyer, J. *J. Chem. Phys.* **2005**, *122*, 184306.

(67) Dreyer, J. *Int. J. Quantum Chem.* **2005**, *104*, 782.

(68) Huse, N.; Bruner, B. D.; Cowan, M. L.; Dreyer, J.; Nibbering, E. T. J.; Miller, R. J. D.; Elsaesser, T. *Phys. Rev. Lett.* **2005**, *95*, 147402.

(69) Dwyer, J. R.; Dreyer, J.; Nibbering, E. T. J.; Elsaesser, T. *Chem. Phys. Lett.* **2006**, *432*, 146.

(70) Dreyer, J. *J. Chem. Phys.* **2007**, *127*, 054309.

(71) Elsaesser, T.; Huse, N.; Dreyer, J.; Dwyer, J. R.; Heyne, K.; Nibbering, E. T. J. *Chem. Phys.* **2007**, *341*, 175.

(72) Rey, R.; Møller, K. B.; Hynes, J. T. *Chem. Rev.* **2004**, *104*, 1915.

(73) Skinner, J. L. *Theor. Chem. Acc.* **2011**, *128*, 147.

(74) Jarzeba, W.; Walker, G. C.; Johnson, A. E.; Barbara, P. F. *Chem. Phys.* **1991**, *152*, 57.

(75) Rosenthal, S. J.; Xiaoliang, X.; Mei, D.; Fleming, G. R. *J. Chem. Phys.* **1991**, *95*, 4715.

(76) Horng, M. L.; Gardecki, J. A.; Papazyan, A.; Maroncelli, M. *J. Phys. Chem.* **1995**, *99*, 17311.

(77) Hercules, D. M.; Rogers, L. B. *Spectrochim. Acta* **1958**, *15*, 398.

(78) Moffitt, W. *J. Chem. Phys.* **1954**, *22*, 320.

(79) Johnson, J. R.; Jordan, K. D.; Plusquellic, D. F.; Pratt, D. W. *J. Chem. Phys.* **1990**, *93*, 2258.

(80) Magnes, B.-Z.; Strashnikova, N. V.; Pines, E. *Isr. J. Chem.* **1999**, *39*, 361.

(81) Knochenmuss, R.; Muino, P. L.; Wickleder, C. *J. Phys. Chem.* **1996**, *100*, 11218.

(82) Fleisher, A. J.; Morgan, P. J.; Pratt, D. W. *J. Chem. Phys.* **2009**, *131*, 211101.

(83) Yoshino, R.; Hashimoto, K.; Omi, T.; Ishiuchi, S.; Fujii, M. *J. Phys. Chem. A* **1998**, *102*, 6227.

(84) Matsumoto, Y.; Ebata, T.; Mikami, N. *J. Chem. Phys.* **1998**, *109*, 6303.

(85) Matsumoto, Y.; Ebata, T.; Mikami, N. *J. Phys. Chem. A* **2001**, *105*, 5727.

(86) Saeki, M.; Ishiuchi, S.; Sakai, M.; Fujii, M. *J. Phys. Chem. A* **2001**, *105*, 10045.

(87) Ebata, T.; Kouyama, K.; Mikami, N. *J. Chem. Phys.* **2003**, *119*, 2947.

(88) Kouyama, K.; Miyazaki, M.; Mikami, N.; Ebata, T. *J. Chem. Phys.* **2006**, *124*, 054315.

(89) Salman, S. R. *Org. Magn. Reson.* **1984**, *22*, 385.

(90) Humphrey, S. J.; Pratt, D. W. *Chem. Phys. Lett.* **1996**, *257*, 169.

(91) Lark, P. D.; Orr, B. J.; Rhoades, G. F. *Aust. J. Chem.* **1975**, *28*, 1417.

(92) Kovács, A.; Varga, Z. *Coord. Chem. Rev.* **2006**, *250*, 710.

(93) Matsumoto, Y.; Ebata, T.; Mikami, N. *J. Mol. Struct.* **2000**, *552*, 257.

(94) Lippert, E. *Z. Naturforsch., A: Phys. Sci.* **1955**, *10*, 541.

(95) Mathies, R.; Albrecht, A. C. *J. Chem. Phys.* **1974**, *60*, 2500.

(96) Abe, T.; Amako, Y.; Nishioka, T.; Azumi, H. *Bull. Chem. Soc. Jpn.* **1966**, *39*, 845.

(97) Riddick, J. A.; Bunger, W. B.; Sakano, T. K. *Organic Solvents: Physical Properties and Methods of Purification*; John Wiley & Sons: New York, 1986.